

# Construction and use of an adaptive optics two-photon microscope with direct wavefront sensing

Pantong Yao<sup>1</sup>, Rui Liu<sup>2</sup>, Thomas Broggini<sup>2</sup>, Martin Thunemann<sup>3</sup> & David Kleinfeld <sup>1,2,4</sup> 

## Abstract


Two-photon microscopy, combined with the appropriate optical labelling, enables the measurement and tracking of submicrometer structures within brain cells, as well as the spatiotemporal mapping of spikes in individual neurons and of neurotransmitter release in individual synapses. Yet, the spatial resolution of two-photon microscopy rapidly degrades as imaging is attempted at depths of more than a few scattering lengths into tissue, i.e., below the superficial layers that constitute the top 300–400  $\mu\text{m}$  of the neocortex. To obviate this limitation, we shape the focal volume, generated by the excitation beam, by modulating the incident wavefront via guidestar-assisted adaptive optics. Here, we describe the construction, calibration and operation of a two-photon microscope that incorporates adaptive optics to restore diffraction-limited resolution at depths close to 900  $\mu\text{m}$  in the mouse cortex. Our setup detects a guidestar formed by the excitation of a red-shifted dye in blood serum, used to directly measure the wavefront. We incorporate predominantly commercially available optical, optomechanical, mechanical and electronic components, and supply computer-aided design models of other customized components. The resulting adaptive optics two-photon microscope is modular and allows for expanded imaging and optical excitation capabilities. We demonstrate our methodology in the mouse neocortex by imaging the morphology of somatostatin-expressing neurons that lie 700  $\mu\text{m}$  beneath the pia, calcium dynamics of layer 5b projection neurons and thalamocortical glutamate transmission to L4 neurons. The protocol requires ~30 d to complete and is suitable for users with graduate-level expertise in optics.

## Key points

- The resolution of two-photon microscopy degrades when imaging deep into tissue, limiting its effectiveness beyond the superficial layer of neocortex. To overcome this limitation, the authors describe the construction and operation of a two-photon microscope that incorporates adaptive optics to restore diffraction-limited resolution for imaging structure and function in deep layers.
- The red-shifted dye cyanine 5.5-conjugated 2,000 kDa dextran is readily delivered to the blood serum and serves as a guidestar for adaptive optics.

## Key references

Liu, R. et al. *Nat. Methods* **16**, 615–618 (2019): <https://doi.org/10.1038/s41592-019-0434-7>

<sup>1</sup>Neurosciences Graduate Program, University of California San Diego, La Jolla, CA, USA. <sup>2</sup>Department of Physics, University of California San Diego, La Jolla, CA, USA. <sup>3</sup>Department of Biomedical Engineering, Boston University, Boston, MA, USA. <sup>4</sup>Department of Neurobiology, University of California San Diego, La Jolla, CA, USA.  e-mail: [dk@physics.ucsd.edu](mailto:dk@physics.ucsd.edu)

## Introduction

Two-photon laser scanning microscopy<sup>1,2</sup> (TPLSM) can image through the murine brain with cellular-to-subcellular resolution and currently provides much of the functional data to decipher how the complex dynamics of neuronal activity encodes sensory input and guides subsequent behavior<sup>3</sup>. With a variety of organic and genetically encoded biosensors<sup>4</sup>, TPLSM permits investigators to record neuronal activity via calcium dynamics<sup>5</sup>, neurotransmitter release<sup>6,7</sup> and voltage signaling<sup>8</sup>. Imaging methods, in contrast to multisite electrodes<sup>9,10</sup>, report the areal organization of the recorded neuronal activity in relation to both real-space coordinates and functional coordinates, e.g., as those used for the visual system<sup>11</sup>. Spatial information may be further used to align the measured neuronal activity with the patterns of gene expression, acquired *ex vivo*, to enable the study of neuronal dynamics in relation to molecularly defined cell types<sup>12</sup>.

The spatial resolution and the signal-to-background ratio of TPLSM degrades with increasing imaging depth. Inhomogeneities in brain tissue and refractive index mismatches through the preparation will aberrate the wavefront of the excitation beam and lead to an enlarged focus with diminished focal intensity (Fig. 1a,b). To counteract the optical aberrations, adaptive optics TPLSM (AO-TPLSM) integrates a phase modulator, i.e., a deformable mirror (DM) or spatial light modulator (SLM), to the conventional TPLSM to compensate the distortion of the wavefront<sup>13</sup> (Fig. 1c). The compensation can be determined by either direct measurement of the distorted wavefront via a wavefront sensor<sup>14–16</sup> (Figs. 1d and 2) or by inferring it indirectly from the acquired signals<sup>17–21</sup>. A recent review comprehensively covered various essential topics in adaptive optics (AO), from the general principles, phase modulation device, wavefront

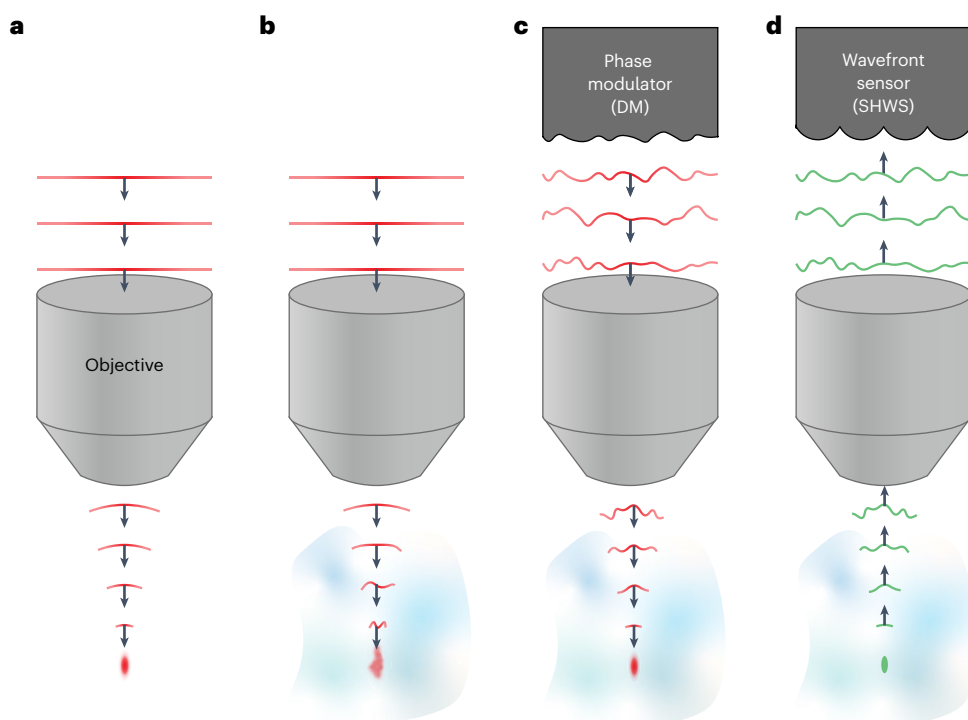


**Fig. 1 | Concepts of AOs and wavefront sensing.** **a**, A schematic diagram illustrating the propagating wavefront of the excitation beam in an aberration-free imaging system in which the beam is focused as a diffraction-limited spot. **b**, Aberrated wavefront as it propagates through the inhomogeneous imaging sample, resulting in an enlarged and distorted focus. **c**, Compensating the aberration by the phase modulator to recover the diffraction-limited focus. **d**, Acquiring the desired wavefront for the phase modulator by direct wavefront sensing of the aberrated wavefront that generates by a point source in the sample.

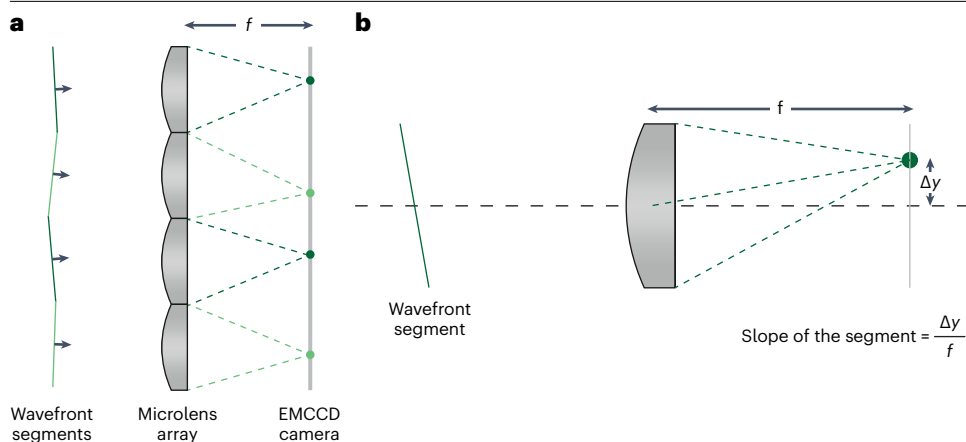


**Fig. 2 | Concepts of Shack–Hartmann wavefront sensing.** **a**, Diagram showing that the aberrated wavefront is split into segments by the lens array and focus on the EMCCD. **b**, Diagram demonstrating that the wavefront can be estimated by calculating the slope of each segment based on the deflection of the focal spot.  $\Delta y$ , the distance of the deflected spot from the central axis of the microlens;  $f$ , the focal length of a microlens.

sensing method and control strategies, to their applications in diverse fields, including microscopy, astronomy and vision science<sup>13</sup>.

## Overview of the procedure

Despite its advantages in neuroscience research, implementing AO-TPLSM presents challenges. Here, we provide a comprehensive guide to construct the hardware and perform AO-TPLSM imaging in a relatively straightforward manner. We share the design of our system (Figs. 3 and 4) in terms of assembly drawings for all components (Supplementary Data 1). We use commercially available parts as much as possible (Tables 1–3) and, for the customized parts, detailed drawings and computer aided design models are supplied (Table 4 and Supplementary Data 2). We have also included the Zemax file in our supplementary materials for users who wish to modify or customize the system (Supplementary Data 3). We present illustrated step-by-step instructions (Fig. 5) for the construction (Steps 1–22 and Supplementary Data 1), alignment (Steps 23–42), calibration (Steps 43–53) and quality control (Steps 54 and 65). The custom MATLAB codes for calibrating and operating the AO-TPLSM system are supplied (Supplementary Software). We provide details of the preparation of the fluorescent molecule, cyanine 5.5-conjugated 2,000 kDa dextran (Cy5.5–dextran), that underlies the guidestar (Steps 66–78). Lastly, we provide example demonstrations of the procedure to perform in vivo imaging experiments with AO corrections (Steps 79–85).

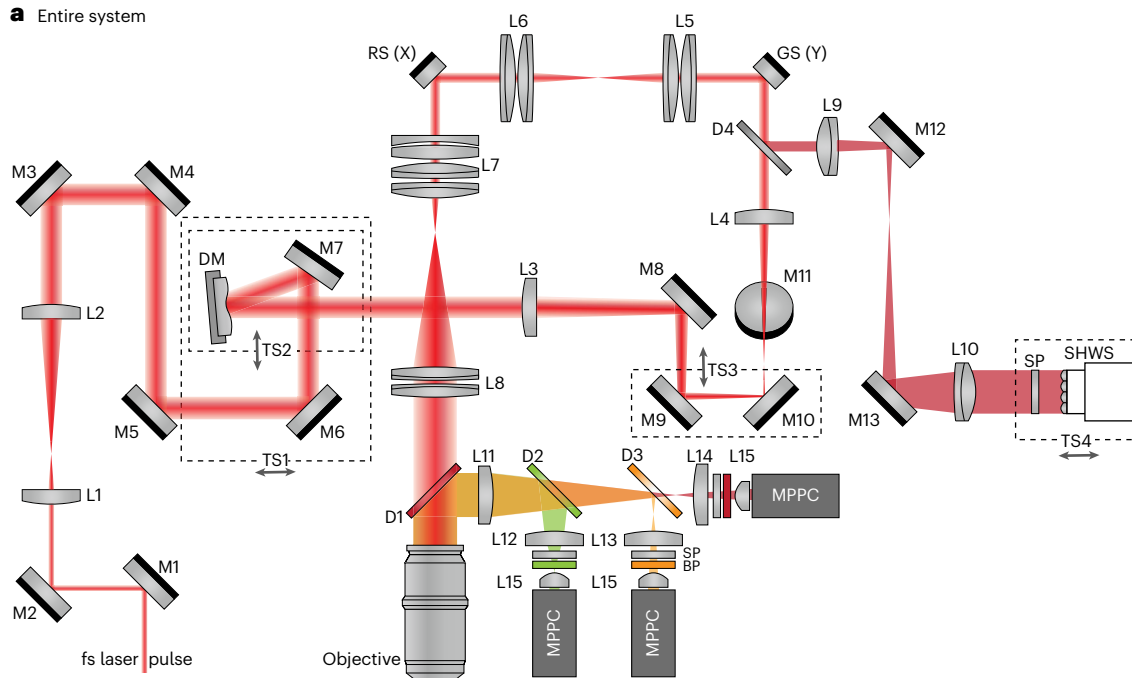
## System design

Like a conventional TPLSM, AO-TPLSM contains an excitation path to focus the excitation beam on the preparation, and a collection path that couples the light emitted at the focus to the photon detectors, i.e., multipixel photon counters (MPPCs) or photomultiplier tubes (Fig. 3a). A pair of the scanners that are conjugating to the rear pupil plane of the objective in the excitation path scans the focus across the preparation during the acquisition of an image. An image frame is constructed from the intensity signal as a function of the scanner angles.

Image quality, including the spatial resolution and signal-to-background ratio, is largely determined by the quality of the focus, and is characterized by the point spread function (PSF). The goal of AO-TPLSM is to compensate for the aberrated wavefront of the excitation beam to achieve a nondistorted PSF (Fig. 1c). The shape of the aberrated wavefront,  $W$ , can be expressed as a sum of Zernike modes, the polynomials labeled  $Z_n^m$  with azimuthal frequency  $m$  and radial order  $n$ , weighted by coefficients  $a_n^m$  where

$$W = \sum_{n=0}^{\infty} \sum_{m=-n}^n a_n^m Z_n^m.$$

**a** Entire system



**b** Descan pathway for direct sensing

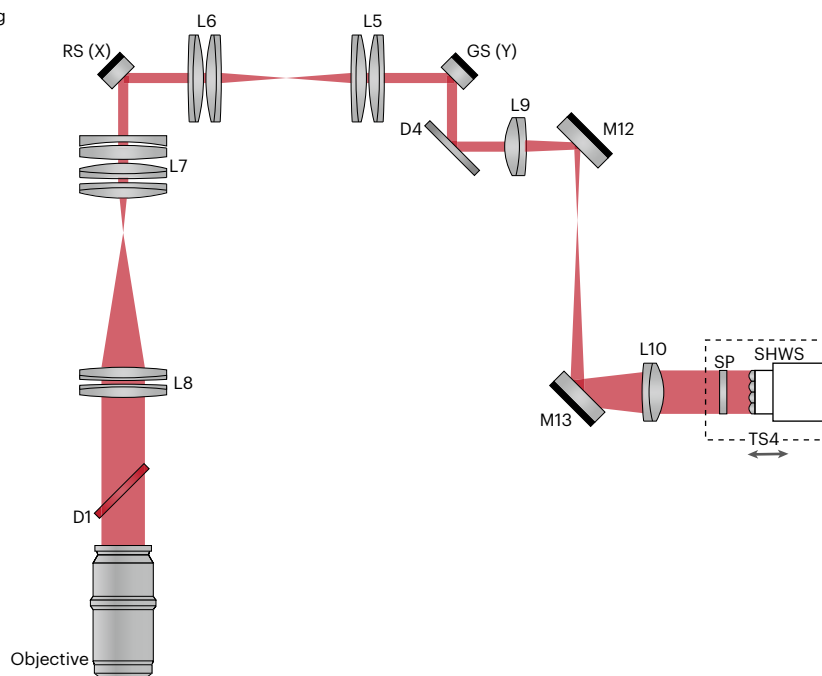


**Fig. 3 | Schematic diagram of AO-TPLSM. a**, A schematic diagram of the entire system showing optics and beam path of the AO-TPLSM. TS, translational stage; M, mirror; L, lens; D, dichroic mirror; SP, shortpass filter; BP, bandpass filter;

GS, galvo scanner; Y, Y-scanner; RS, resonant scanner; X, X-scanner; fs laser, femtosecond laser. **b**, Schematic diagram showing only the optics that are involved in descanning of the guidestar signal.

In our implementation of AO-TPLSM (Fig. 3a), we integrate a DM to the excitation path, whose reflective surface is a membrane that can be deformed to closely approximate a sum of Zernike modes  $Z_n^m$ , each with magnitude  $a_n^m$ , by a group of actuators. This changes the optical

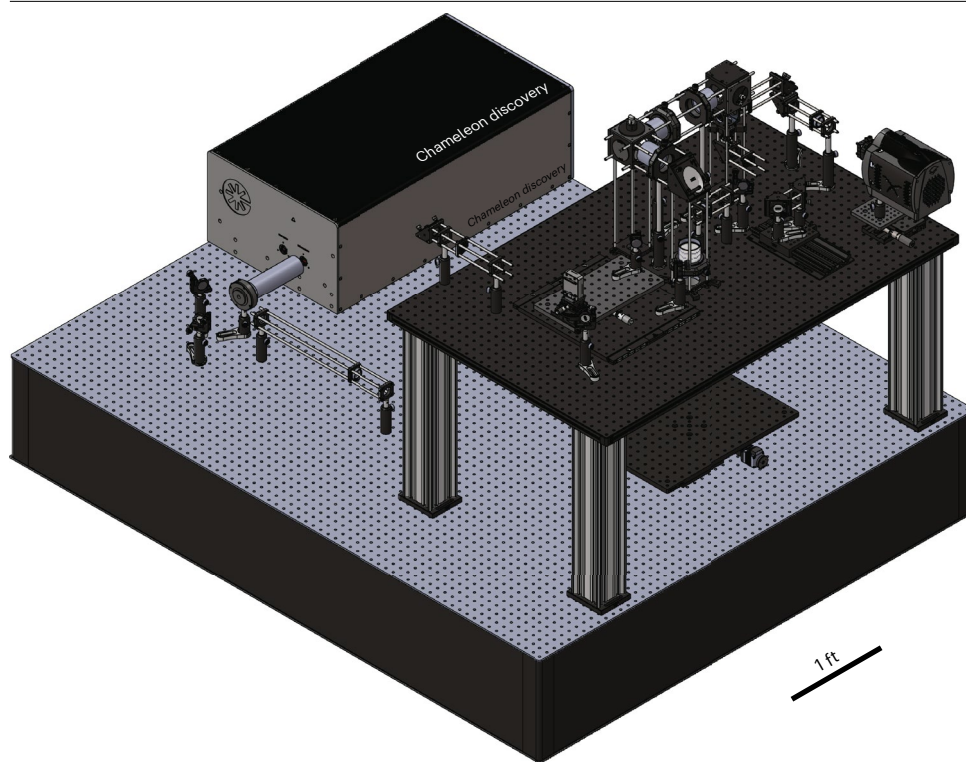


**Fig. 4 | Implementation example of AO-TPLSM.** Computer model of AO-TPLSM. Detailed technical drawings are provided in Supplementary Data 1.

path length and thus introduces a known, corrective distortion to the wavefront (Fig. 1c). To fully utilize the surface of the DM, the excitation beam is expanded to fill the aperture of the DM using a pair of lenses (L1 and L2) between the laser and the DM. The pattern on the DM is imaged to the rear pupil plane of the objective, i.e., the two planes are conjugate (Fig. 6). This is achieved by a second pair of lenses (L3 and L4) between the DM and the Y-scanner, that form a four-times focal length (4-f) relay to conjugate the DM with the Y-scanner and demagnify the image of the DM. The X- and Y-scanners are conjugated to each other via another 4-f relay (L5 and L6), and to the pupil plane by the scan lens (L7) and tube lens (L8). Each of L5, L6 and L8 is composed of a pair of achromatic doublets, effectively reducing spherical aberration and coma within the imaging system, and L7 consists of a plano-concave lens, a bi-convex lens and two achromatic doublets to minimize the field curvature and astigmatism.

To determine the desired wavefront for the DM, the wavefront from the descanned point source in the sample, known as the guidestar signal, which represents the aberration, is measured by direct wavefront sensing (Fig. 1d). This is achieved by a Shack–Hartmann wavefront sensor (SHWS), consisting of a microlens array and an electron multiplying charge-coupled device (EMCCD) that is located at the focal plane of the microlens array (Fig. 2a). The local tilt of the aberrated wavefront, segmented by the microlens array, will deflect focused spots on the EMCCD away from their center and the angles of the deflections are used to estimate the wavefront from the guidestar signal (Fig. 2b). The guidestar signal propagates to the SHWS through the descan path (Fig. 3b), which shares lenses L5–L8 and the scanners with the excitation beam. To separate the guidestar light from the excitation beam, a dichroic mirror (D4) is employed to reflect the guidestar light to the wavefront sensing path. The SHWS also needs to be conjugated to the rear pupil of the objective, like the case for the DM, and another 4-f set of relay lenses (L9 and L10) is introduced to conjugate the microlens array with the Y-scanner.

**Table 1 | Optical components for AO-TPLSM**

Item		Part no.	Description	Vendor	Quantity
Lens	4-f scanner	AC508-150-B	$f = 150.0$ mm, $\varnothing 2''$ Achromatic Doublet, antireflective coating (ARC): 650–1,050 nm	Thorlabs	4
	Scan lens	AC508-150-B	$f = 150.0$ mm, $\varnothing 2''$ Achromatic Doublet, ARC: 650–1,050 nm	Thorlabs	2
		LB1199-B	N-BK7 Bi-Convex Lens, $\varnothing 2''$ , $f = 200.0$ mm, ARC: 650–1,050 nm	Thorlabs	1
		KPC070AR.16	Plano-Concave Lens, N-BK7, 50.8 mm diameter, $-200$ mm effective focal length (EFL), 650–1,000 nm	Newport	1
	Tube lens	ACT508-500-B	$f = 500.0$ mm, $\varnothing 2''$ Achromatic Doublet, ARC: 650–1,050 nm	Thorlabs	1
	Fluorescent collection	A240-A	$f = 8.00$ mm, NA = 0.5, Unmounted Rochester Aspheric Lens, ARC: 350–700 nm	Thorlabs	3
		LA1765-A	N-BK7 Plano-Convex Lens, $\varnothing 30.0$ mm, $f = 75.0$ mm, ARC: 350–700 nm	Thorlabs	1
		LA1805-A	N-BK7 Plano-Convex Lens, $\varnothing 1''$ , $f = 30.0$ mm, ARC: 350–700 nm	Thorlabs	2
		LA1027-A	N-BK7 Plano-Convex Lens, $\varnothing 1''$ , $f = 35.0$ mm, ARC: 350–700 nm	Thorlabs	1
	Beam expander	LA1805-B	N-BK7 Plano-Convex Lens, $\varnothing 1''$ , $f = 30$ mm, ARC: 650–1,050 nm	Thorlabs	1
		LA1484-B	N-BK7 Plano-Convex Lens, $\varnothing 1''$ , $f = 300$ mm, ARC: 650–1,050 nm	Thorlabs	1
	Beam compressor	KPX117AR.18	Plano-Convex Lens, N-BK7, 25.4 mm diameter, 450 mm EFL, 1,000–1,550 nm	Newport	1
		KPX100AR.18	Plano-Convex Lens, N-BK7, 25.4 mm diameter, 150 mm EFL, 1,000–1,550 nm	Newport	1
	Beam expander for wavefront sensing	AC254-125-A	$f = 125$ mm, $\varnothing 1''$ Achromatic Doublet, ARC: 400–700 nm	Thorlabs	1
		AC254-200-A	$f = 200$ mm, $\varnothing 1''$ Achromatic Doublet, ARC: 400–700 nm	Thorlabs	1
Objective		XLPLN25XSVM2	Multiphoton Excitation Objectives	Olympus	1
Microlens array		#64-483	Microlens Array $10 \times 10$ mm, 500 $\mu$ m pitch, $0.25^\circ$ divergence	Edmund	1
Elliptical mirror		PFE20-P01	2" Protected Silver Elliptical Mirror, 450 nm–20 $\mu$ m	Thorlabs	1
Reflecting mirror		PF10-03-P01-10	$\varnothing 1''$ Protected Silver Mirror, 10 pack	Thorlabs	2
Beamsplitter	Wavefront sensing	FF775-DiO1-25 $\times$ 36	775 nm edge BrightLine multiphoton single-edge dichroic beamsplitter	Semrock	1
	Fluorescent collection	FF775-DiO1-25 $\times$ 36	775 nm edge BrightLine multiphoton single-edge dichroic beamsplitter	Semrock	1
		FF665-DiO2-35 $\times$ 37-EB	665 nm edge BrightLine multiphoton single-edge dichroic beamsplitter	Semrock	1
		FF552-DiO2-25 $\times$ 36	552 nm edge BrightLine single-edge standard epi-fluorescence dichroic beamsplitter	Semrock	1
		FF662-FDiO1-25 $\times$ 36	662 nm edge BrightLine single-edge image-splitting dichroic beamsplitter	Semrock	1
Filter	Fluorescent collection	FF01-530/55-25	530/55 nm BrightLine single-band bandpass filter	Semrock	1
		FF01-593/46-25	593/46 nm BrightLine single-band bandpass filter	Semrock	1
		FF01-708/75-25	708/75 nm BrightLine single-band bandpass filter	Semrock	1
		FF01-790/SP-25	790 nm blocking edge BrightLine multiphoton short-pass emission filter	Semrock	3
	Wavefront sensing	FF01-790/SP-25	790 nm blocking edge BrightLine multiphoton short-pass emission filter	Semrock	1

It is essential to conjugate the X-scanner, Y-scanner, DM and SHWS to the rear pupil of the objective for successful aberration correction (Steps 23–42; Figs. 7–9). Conjugating these components is not trivial since corrections to the position of one component may break the conjugation between other components. To minimize this difficulty, our system is designed to orthogonalize the conjugation procedure from alignment. For example, the DM is mounted on a translational stage (TS1) with a pair of mirrors (M6 and M7) so that sliding TS1 along the optical axis minimally affects the overall alignment of the excitation beam. A mirror pair on the TS3 stage are introduced to adjust the optical path between the L3 and L4 lenses so that the collimation of the excitation beam can be adjusted without affecting the conjugation (Fig. 6). The critical dimensions for conjugation, noted in the assembly drawing (Supplementary Data 1), should be carefully followed. Further, we optimized the assembly sequence so that conjugation at the final steps does not affect conjugation of components early in the assembly process.



**Table 2 | Electronics and opto-electronics for AO-TPLSM**

Item	Description	Vendor	Part number	Quantity
EMCCD	For SHWS	Andor	DU-888U3-CS0-BV	1
Deformable mirror	DM97-15; high speed dm option; trigger option	Alpao	DM97-15	1
Translation stage	50 mm (1.97") TravelMax translation stage, 1/4"-20 taps	Thorlabs	LNR502	3
Translation stage controller	Three-channel controller and knob box for 2" stages with stepper motor	Thorlabs	MCM3003	1
Resonant scanner	5 mm, 8 kHz, 26 optical degree, silver	Cambridge Technology	CRS8K	1
Galvo scanner	6 mm, 40 optical degree, silver	Cambridge Technology	8315K	1
E-O modulator	(Optional) Pockel cell for excitation laser power control	ConOptics	350-105-02	1
E-O modulator driver		ConOptics	302RM	1
MPPC	Optical measurement modules for low-level-light detection, Analog output	Hamamatsu	C13366-3050GA	3
MPPC amplifier	350 MHz preamplifier	Stanford research system	SR445A	2
Laser shutter	LS6 6 mm laser shutter	Vincent Associates	LS6	1
Laser shutter driver	VCM-D1 shutter driver	Vincent Associates	VCM-D1	1
PXIe-1073	PXI chassis	National Instruments	781163-01	1
	NI PCIe-8361: 1 port MXI-express interface	National Instruments	779504-01	1
	MXI-express cable	National Instruments	779500-03	1
PXIe-7961	PXI FPGA module for FlexRIO	National Instruments	781205-01	1
NI-5734	Digitizer adapter module for FlexRIO	National Instruments	781659-04	1
PXIe-6341	PXI multifunction I/O module	National Instruments	781052-01	2
	Terminal block, model: BNC-2090A	National Instruments	779556-01	2
	SHC68-68-EPM shielded cable, 68-D-type to 68 VHDCI, Offset, 2 m	National Instruments	192061-02	2

## Operational logic

Besides aberrations that are caused by brain tissue, the imaging system per se aberrates the excitation beam because of imperfections in the optics, misalignments in the microscope and the aberrations induced by the cover glass of the cranial window. These are referred to as system aberrations. To achieve the best image quality, as well as to maximize the imaging depth, both sample aberrations and system aberrations need to be corrected.

To determine the wavefront pattern, or phase map, for correcting the sample aberration, we apply the direct wavefront sensing method and measure the wavefront of the descanned guidestar with the SHWS. Conceptually, the guidestar refers to an ideal point source of light in the sample whose wavefront will be aberrated as it propagates through the tissue to the rear pupil (Fig. 1d). On the basis of the reversibility of optical wave propagation, applying the same aberrated wavefront at the pupil generates a diffraction-limited focus in the tissue (Fig. 1c). In practice, as a two-photon excited fluorescence naturally produces a confined light source, we used the emitted light of two-photon excited Cy5.5-dextran in the brain microvessels as the guidestar<sup>16,22</sup>. Cy5.5-dextran is a red-shifted dye that is bright, inexpensive to produce, apparently nontoxic and readily delivered to the vessels by either retro-orbital injection<sup>23</sup> or tail vein injection. Unlike directly injecting a dye into a region of the brain<sup>14</sup>, vascular circulation constantly replenishes the guidestar and makes it compatible with transcranial windows<sup>24</sup> as well as 'open' cranial windows<sup>25</sup> for chronic imaging. Steps 66–78 describe the procedure to synthesize 3% (wt/vol) 2000 kDa Cy5.5-dextran, which will be used for generating the guidestar signal for sample aberration correction in vivo.

To compute the DM pattern based on the SHWS images from the guidestar, it is critical to establish the relation between the DM pattern, in terms of its Zernike modes, to the SHWS, in term of the deflection of the spots from each microlens in the array. This is achieved by AO calibration (Steps 43–49; Figs. 10 and 11), in which we place a mirror at the pupil level to map the DM to the SHWS and record the corresponding pattern of the deflected spots on SHWS when each of the individual Zernike modes is displayed by the DM.

**Table 3 | Opto-mechanics for AO-TPLSM**

Item	Part number	Description	Vendor	Quantity
Optical post	SP-2	Optical post, 2.0", height, 0.5", diameter, 8-32 and 1/4-20 thread	Newport	1
Kinematic cage cube platform	B4C	Kinematic cage cube platform for C4W/C6W	Thorlabs	1
Base adapter	BE1-P5	Ø1.25" Studded pedestal base adapter, 1/4"-20 thread, 5 pack	Thorlabs	3
Cage cube	C4W	30 mm Cage cube	Thorlabs	1
Clamping fork	CF125C-P5	Clamping fork, 1.24" counterbored slot, 1/4"-20 captive screw, 5 pack	Thorlabs	3
Pedestal post table clamp	CL8	Ø1" and Ø1.5" Pedestal post table clamp	Thorlabs	4
Cage plate	CP08	SM1-threaded 30 mm cage plate with flexure clamping, 1 retaining ring, 8-32 tap	Thorlabs	5
Cage system Iris	CP20S	30 mm Cage system iris diaphragm (Ø0.8–Ø20 mm)	Thorlabs	5
Cage plate	CP33	SM1-threaded 30 mm cage plate, 0.50" thick, 2 retaining rings, 8-32 tap	Thorlabs	8
Cage plate	CPTS10	Cage plate to Ø1/2" post adapter, 10 mm post offset, imperial thumbscrew	Thorlabs	1
Mounting plate	CPVMP	Vertical cage system mounting plate for 30 mm and 60 mm cage systems	Thorlabs	3
Cage rotation	CRM1T	Cage rotation mount for Ø1" optics, sm1 threaded, 8-32 tap	Thorlabs	1
Lens mount	CXY1	30 mm Cage system, xy translating lens mount for Ø1" optics	Thorlabs	1
Translating lens mount	CXY2	60 mm Cage system translating lens mount for Ø2" optics	Thorlabs	4
Drop-in 30 mm cage mount	DCP1	Drop-in 30 mm cage mount, flexure lock, sm1 threaded, 0.40" thick, 2 retaining rings	Thorlabs	1
Cage assembly rod	ER05-P4	Cage assembly rod, 1/2" long, Ø6 mm, 4 pack	Thorlabs	1
Cage assembly rod	ER1-P4	Cage assembly rod, 1" long, Ø6 mm, 4 pack	Thorlabs	4
Cage assembly rod	ER2-P4	Cage assembly rod, 2" long, Ø6 mm, 4 pack	Thorlabs	6
Cage assembly rod	ER3-P4	Cage assembly rod, 3" long, Ø6 mm, 4 pack	Thorlabs	1
Cage assembly rod	ER4-P4	Cage assembly rod, 4" long, Ø6 mm, 4 pack	Thorlabs	1
Cage assembly rod	ER6-P4	Cage assembly rod, 6" long, Ø6 mm, 4 pack	Thorlabs	4
Cage assembly rod	ER10	Cage assembly rod, 10" long, Ø6 mm	Thorlabs	12
Cage assembly rod	ER12	Cage assembly rod, 12" long, Ø6 mm	Thorlabs	4
Cage assembly rod	ER18	Cage assembly rod, 18" long, Ø6 mm	Thorlabs	8
Rectangular filter mount	FFM1	30 mm Cage-compatible rectangular filter mount	Thorlabs	1
Large goniometer	GNL18	Large goniometer, 1.75" distance to point of rotation, ±5°	Thorlabs	1
45° Mirror mount	H45	45° Mirror mount for Ø1" optics	Thorlabs	1
Kinematic mirror mount	KCB1C	Right-angle kinematic mirror mount with smooth cage rod bores, 30 mm cage system and SM1 compatible, 8-32 and 1/4"-20 mounting holes	Thorlabs	6
Kinematic elliptical mirror mount	KCB2EC	Right-angle kinematic elliptical mirror mount with smooth cage rod bores, 60 mm cage system and SM2 compatible, 8-32 and 1/4"-20 mounting holes	Thorlabs	1
Kinematic mirror mount	KM100	Kinematic mirror mount for Ø1" optics	Thorlabs	6
Compact kinematic mirror Mount	KMS	Compact kinematic mirror mount, 8-32 taps for post mounting	Thorlabs	1
Light-tight blank cover plate	LB1C	Light-tight blank cover plate for 60 mm cage cube, 1/4"-20 tap	Thorlabs	2
Cage cube	LC6W	60 mm Cage cube	Thorlabs	2
Mounting bracket	LCP01B	60 mm Cage mounting bracket	Thorlabs	3
30 mm to 60 mm cage plate adapter	LCP33	30 mm to 60 mm Cage plate adapter, 8-32 tap	Thorlabs	2
XY adapter plate	LNR50P3	XY Adapter plate for LNR50 TravelMax stages, imperial hole spacings	Thorlabs	2
Aluminum breadboard	MB1218	Aluminum breadboard 12" × 18" × 1/2", 1/4"-20 taps	Thorlabs	1
Aluminum breadboard	MB612F	Aluminum breadboard, 6" × 12" × 1/2", 1/4"-20 taps	Thorlabs	1
Mirror holder	MH25	Mirror holder for Ø1" optics 2.5–6.1 mm thick	Thorlabs	1
Aluminum breadboard	MSB46	4" × 6" × 3/8" Mini-series aluminum breadboard, 8-32 and 1/4"-20 high-density taps	Thorlabs	1
UltraLight breadboard	PBG3048F	UltraLight breadboard, 30" × 48" × 0.98", 1/4"-20 taps	Thorlabs	1
Post holder	PH1.5	Ø1/2" Post holder, spring-loaded hex-locking thumbscrew, L = 1.5"	Thorlabs	2
Post holder	PH2-P5	Ø1/2" Post holder, spring-loaded hex-locking thumbscrew, L = 2", 5 Pack	Thorlabs	1
Post holder	PH3-P5	Ø1/2" Post holder, spring-loaded hex-locking thumbscrew, L = 3", 5 Pack	Thorlabs	2
Post holder	PH4-P5	Ø1/2" Post holder, spring-loaded hex-locking thumbscrew, L = 4", 5 Pack	Thorlabs	1



**Table 3 (continued) | Opto-mechanics for AO-TPLSM**

Item	Part number	Description	Vendor	Quantity
High-precision rotation mount	PR01	High-precision rotation stage, 1/4"-20 and 6-32 taps	Thorlabs	1
Translation stage with standard micrometer	PT1	1" Translation stage with standard micrometer, 1/4"-20 taps	Thorlabs	1
Post collar	R2T	Thin slip-on post collar for Ø1/2" posts, 5 pack	Thorlabs	2
Right-angle end clamp	RA180	Right-angle end clamp for Ø1/2" posts, 1/4"-20 stud and 3/16" hex	Thorlabs	1
Adaptor	SM1A39	Adapter with external C-mount threads and external SM1 threads	Thorlabs	1
Lens tube	SM1L03	SM1 lens tube, 0.30" thread depth, one retaining ring included	Thorlabs	5
End cap	SM2CP2	Externally SM2-threaded end cap	Thorlabs	4
Lens tube	SM2L15	SM2 lens tube, 1.5" thread depth, one retaining ring included	Thorlabs	3
Lens tube	SM2L20	SM2 lens tube, 2" thread depth, one retaining ring included	Thorlabs	1
Retaining ring	SM2RRC	Extra-thick sm2 (2.035"-40) threaded retaining ring	Thorlabs	1
Large-area translation stage	TBB1212	Large-area translation stage, 12" × 13.66"	Thorlabs	1
Optical post	TR1.5	Ø1/2" Optical post, ss, 8-32 setscrew, 1/4"-20 tap, L = 1.5"	Thorlabs	1
Optical post	TR2-P5	Ø1/2" Optical post, ss, 8-32 setscrew, 1/4"-20 tap, L = 2", 5 pack	Thorlabs	1
Optical post	TR3-P5	Ø1/2" Optical post, ss, 8-32 setscrew, 1/4"-20 tap, L = 3", 5 pack	Thorlabs	2
Optical post	TR4	Ø1/2" Optical post, ss, 8-32 setscrew, 1/4"-20 tap, L = 4"	Thorlabs	2
Optical post	TR10	Ø1/2" Optical post, ss, 8-32 setscrew, 1/4"-20 tap, L = 10"	Thorlabs	3
Universal base plate	UBP2	Universal base plate, 2.5" × 2.5" × 3/8"	Thorlabs	2
Extended dovetail baseplate	XR25DR2	Extended dovetail baseplate for stages with 3" wide dovetails, 150 mm	Thorlabs	1
Translation stage	XR50P	50 mm Travel linear translation stage, side-mounted micrometer, 1/4"-20 Taps	Thorlabs	1
Rail	XT95-500	95 mm Construction rail, clear anodized, L = 500 mm	Thorlabs	5
Base plate	XT95P3	Base plate for 95 mm rails	Thorlabs	9
Drop-on rail carriage	XT95RC4	Drop-on rail carriage for 95 mm rails, 4.00" long, 1/4"-20 tapped holes	Thorlabs	3
Rail	XT95SD-250	95 mm One-sided construction rail, black anodized, L = 250 mm	Thorlabs	1
Mounting plate	G061008000	Mounting plate without hole	Digikey	7
Mounting plate	G061010000	Mounting plate 25	Digikey	3
Mounting plate	G061042000	Mounting plate 30	Digikey	9
Mounting plate	G061045000	Mounting plate M35×0.5	Digikey	4
Mounting plate	G061047000	Mounting plate 35	Digikey	1
Corner connector	G061110000	Corner connector 40	Digikey	12
Corner connector	G061120000	Corner connector 80	Digikey	6
Rods	G061207000	Rod 20 mm	Digikey	12
Adjustable prism insert	G063731000	Adjustable prism insert 30	Digikey	4
Retaining rings	G065078000	Retaining rings 1", 2 ea.	Digikey	5

For the system aberrations, an indirect wavefront sensing method is applied to search for the best pattern on the DM that recovers the PSF in the aberration-free sample (Steps 50–53). The pattern on the DM can be considered as a sum of individual Zernike modes. We utilized a gradient-descent algorithm (Supplementary Software) to optimize the coefficient for each Zernike mode by maximizing the emission intensity of a fluorescent solution, under a cover glass<sup>16</sup> (Fig. 12). The procedure starts with a flat pattern displayed on the DM. In each iteration, images are obtained with an individual Zernike mode added to or subtract from the DM pattern that was obtained from prior iterations. The intensity gradient with respect to each Zernike coefficient is determined as the difference between the average intensity of the images taken with the corresponding Zernike mode added versus subtracted. At the end of each iteration, all Zernike coefficients are updated based on the result of the gradient-descent algorithm. After several rounds of iteration, the coefficients of all Zernike modes are found to stabilize at asymptotic values (Fig. 13). This leads to a diffraction-limited PSF in the aberration-free sample (Fig. 14).

**Table 4 | Custom opto-mechanics for AO-TPLSM**

No.	Part name	Quantity	Original part	Notes
1	Main breadboard	1	Thorlabs, PBG3048F	
2	Z-motor adaptor	1	De novo	
3	XY stage breadboard	1	Thorlabs, MB1218	
4	Galvo mounting plate	1	De novo	Quantity:1 (for the galvo–resonant scanner system) Or Quantity:2 (for a galvo–galvo scanning system)
5	Galvo holder (6-mm 8135K X-galvo)	1	De novo	Inform the machinist that Part No. 5/Part No. 5 backup must be able to fit into Part No. 4
5 backup	(Optional) Galvo holder (6-mm 8135K Y-galvo)	1	De novo	Required for the galvo–galvo system Not required for the galvo–resonant scanner system
6	Resonant scanner mounting plate	1	De novo	The information about the SM1 threads can be found here: <a href="https://www.thorlabs.com/newgrouppage9.cfm?objectgroup_id=1524">https://www.thorlabs.com/newgrouppage9.cfm?objectgroup_id=1524</a>
7	Resonant scanner holder	1	De novo	Inform the machinist that the resonant scanner must be able to fit into Part No. 7
8	Extra-thick retaining ring	1	Thorlabs, SM2RRC	
9	Vertical mounting plate	1	Thorlabs, CPVMP	
10	ER11.23	4	Thorlabs, ER12	
11	Objective mounting plate	1	LINOS Microbench, G061008000	
12	MPPC cover	3	Hamamatsu, C13366-3050GA	Take the cover off from the MPPC body
13	MPPC mounting plate	3	LINOS Microbench, G061010001	
14	Dichroic mount (short)	2	De novo	
15	Dichroic mount (long)	2	De novo	
16	Adjustable prism insert	4	LINOS Microbench, G063731000	
17	L11 mounting plate	1	LINOS Microbench, G061042000	
18	Retaining ring (L12, L13, L14)	3	LINOS Microbench, G065078000	
19	Mounting plate (D1)	1	LINOS Microbench, G061042000	
20	DM adaptor	1	De novo	
21	DM breadboard	1	Thorlabs, MB612F	
22	EMCCD breadboard	1	Thorlabs, MSB46	
23	Lens array adaptor	1	De novo	Incorporate rounded corners to the square counterbore
24	DM conjugation tool	1	De novo	

With the system aberration correction complete, we take a calibration pattern of the deflection of spots on the SHWS (Fig. 10c). This serves as a reference that must be matched during the direct-sensing waveform correction. In particular, the calibration pattern could have slightly off-center spots since the descanning pathway will introduce aberration (Fig. 3b).

We encourage the users to calibrate the system regularly, e.g., twice a year for the best performance, including the AO calibration (Steps 43–49) and system aberration calibration (Steps 50–53). We also recommend that the users verify the imaging system after the calibration by correcting a known aberration, introduced by a double-layered cover glass, in fluorescent fiber sample (Steps 54–65). By doing so, any potential problems or challenges can be identified and addressed beforehand, ensuring optimal performance during live imaging experiments.

The sample aberration, as it varies region by region, should be corrected for every field of view during experiment (Steps 79–85). The region in which a single correction achieves substantial improvement in image quality is defined as the isoplanatic patch. The isoplanatic patch size of the mouse brain is at most hundreds of micrometers<sup>14,16,26–28</sup>. In practice, to achieve the best imaging quality, we recommend that the user perform sample aberration correction for each 100  $\mu\text{m}$   $\times$  100  $\mu\text{m}$ , or even 50  $\mu\text{m}$   $\times$  50  $\mu\text{m}$ , field of view and apply the resulting pattern within an axial range of  $\pm 50$   $\mu\text{m}$ .

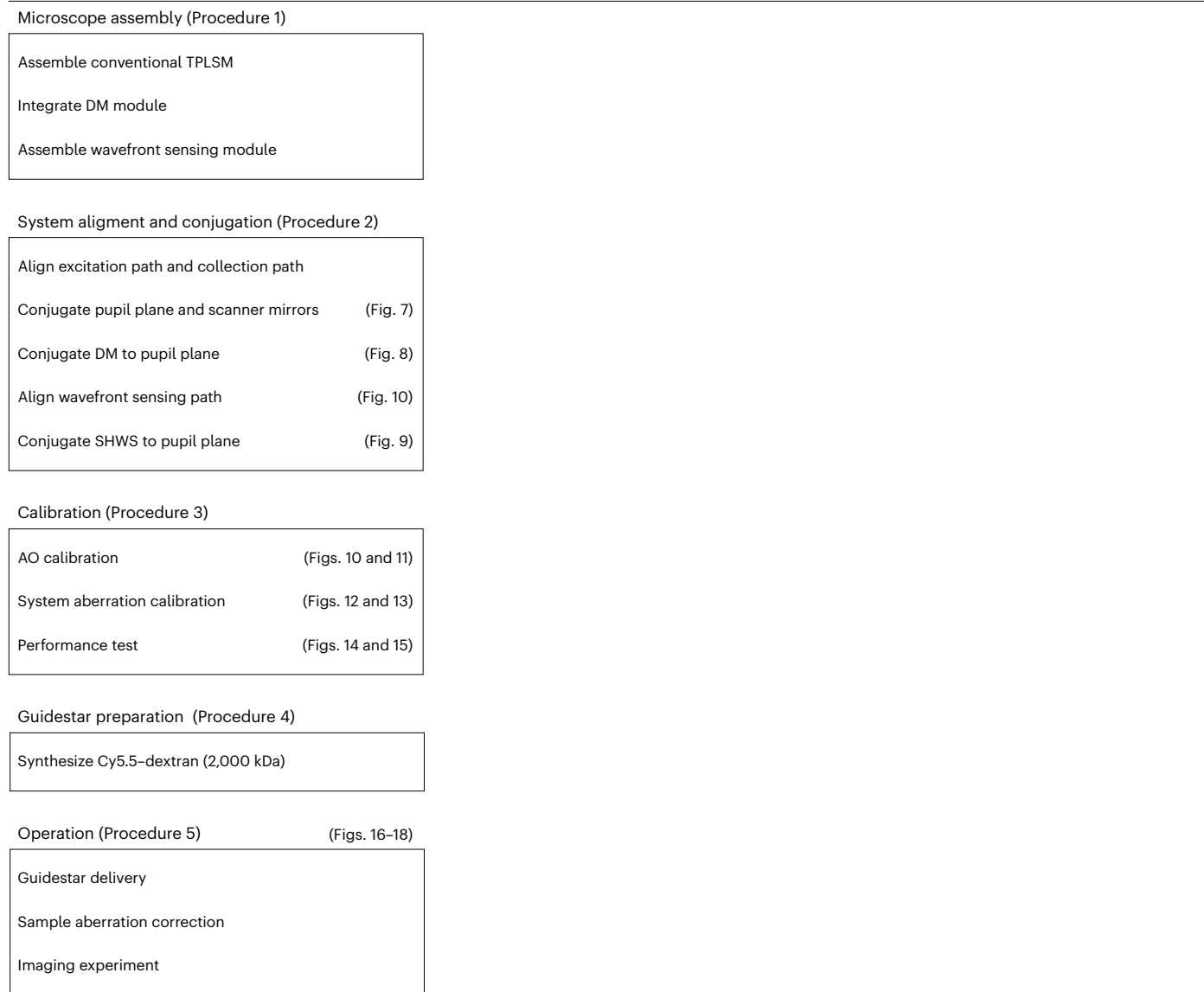


**Fig. 5 | Overview of the procedure.** A flowchart illustrating the essential steps for constructing, aligning and calibrating the AO-TPLSM as well as showing the main steps for conducting an imaging experiment with AO-TPLSM.

## Application of the method

With the capability of correcting the aberration of a given sample, AO-TPLSM could be widely applied to improve the image resolution and signal-to-noise ratio (SNR) during *in vivo* imaging. We previously demonstrated near-diffraction-limited images using direct wavefront sensing from descanned guidestars formed in labeled brain microvessels in awake behaving mice. We resolved soma and fine structures, such as dendrites and individual synaptic spines, up to 850  $\mu\text{m}$  below the pia<sup>16</sup>. Together with the expression of genetically encoded sensors, this approach has been used in the study of cortical deep layers, including the recording of the calcium transients in spines of layer 5b basal dendrites<sup>16</sup> and imaging the glutamate signal from presynaptic boutons and postsynaptic spines during tactile sensing<sup>7</sup>. Besides recording in neocortex, AO-TPLSM has been employed to correct the optical aberrations of the mouse eye for noninvasive retinal imaging at subcellular resolution<sup>29</sup>.

Endoscopic gradient-index (GRIN) lenses extend the optical access to regions that are deep below the pial surface in the brain<sup>12,30,31</sup>. However, the intrinsic aberrations of the GRIN lens cause

# Protocol

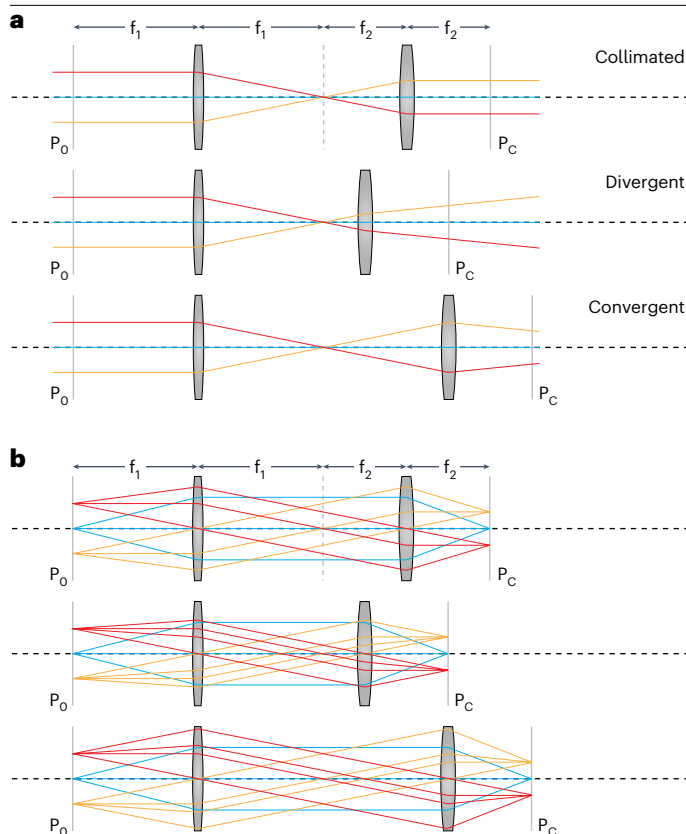


**Fig. 6 | Concepts of collimation and conjugation. a**, Diagram demonstrating that the divergence of the beam passing through a telescope can be controlled by adjusting the distance between the lens pair. **b**, Diagram illustrating the concepts of conjugation. The conjugate of a given plane  $P_0$  is defined as the plane  $P_C$  where the points on  $P_0$  are imaged. Top: a 4- $f$  system that the front focal plane of the first lens and the back focal plane of the second lens are conjugate to each other. Middle and bottom: adjusting the distance between the lenses of a telescope does not change the conjugation of the two focal planes. We applied this feature to the design of the relay between the DM and the scanner to orthogonalize the collimation and conjugation.

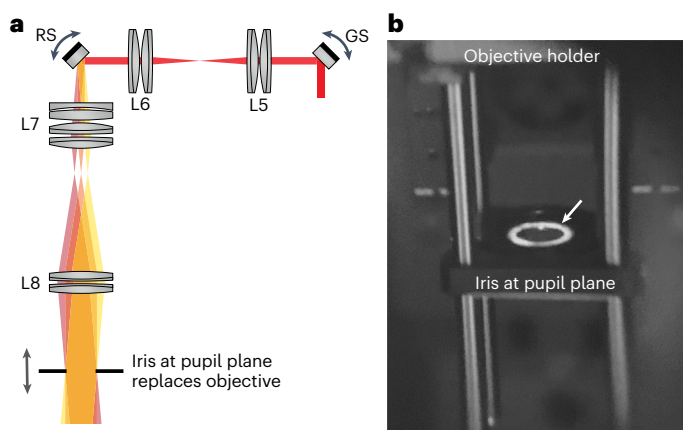


**Fig. 7 | Conjugating the pupil plane with the scanners. a**, Diagram illustrating the objective pupil plane that conjugates to the scanners, relates to Step 36. The objective is replaced by an iris that is located at the pupil plane of the objective. Distinct scanning angles are color coded, and their corresponding beams overlap at the conjugate plane. **b**, Real time image of the iris at the pupil plane taken through the IR viewer. The objective was removed from its holder and an iris was mounted at the pupil plane of the objective. The white arrow points to the edge of the excitation beam, which is concentric with the center of the iris. This indicates that the excitation beam is well aligned with the center of the back aperture. While the scanner is on, no movement of the bright ring should be observed if the iris is conjugated to the scanners.

# Protocol

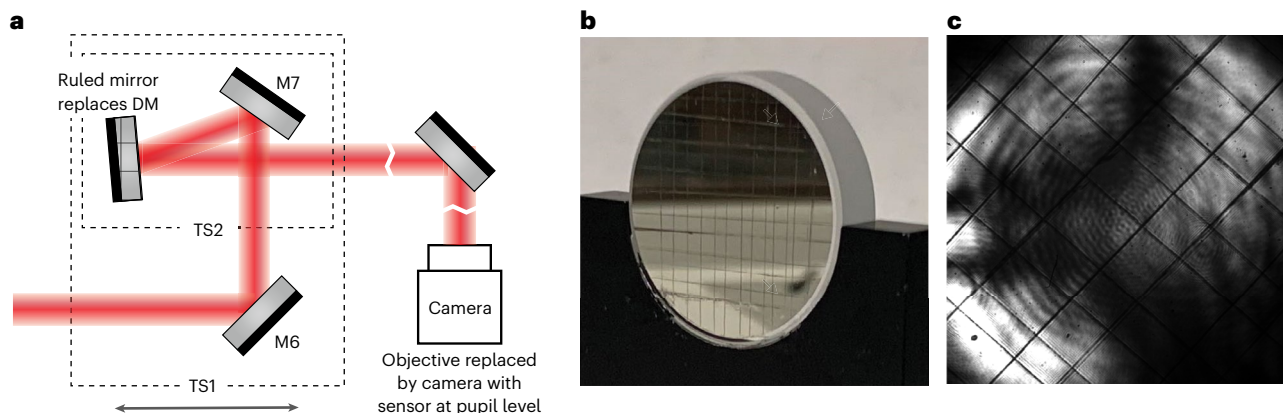


**Fig. 8 | Conjugating the DM to the pupil plane.** **a**, A schematic for finding the DM location along the optical axis that conjugates to the pupil plane, relates to Step 38. The objective is replaced by a camera with its sensor at the pupil plane. The DM is replaced by a mirror with scratches for the camera to image. **b**, Real

item image of the scratched mirror we used to replace the DM. **c**, Image of the scratched mirror taken by the camera at the pupil plane. The sharp grid pattern indicates that the mirror is at the conjugate plane of the pupil.

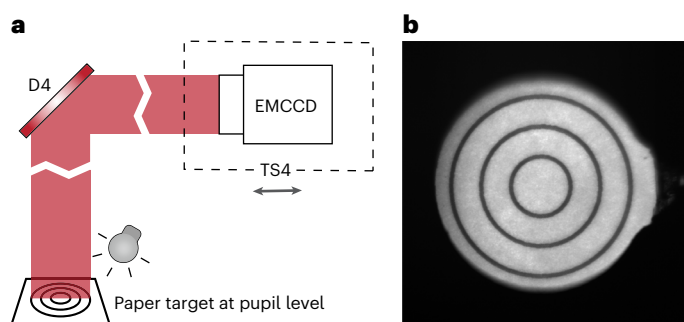


**Fig. 9 | Conjugating SHWS to the pupil plane.** **a**, A schematic showing the setup for finding the plane in the wavefront sensing path that conjugates to the pupil, relates to Step 42. The laser shutter was closed in this step. Another light source, e.g., a flashlight, is needed to illuminate the paper target at the pupil plane. **b**, Sharp image of the target, indicating that the EMCCD sensor is conjugated to the pupil plane.

the imaging resolution to decay dramatically radially and axially and results in a small field of view and narrow depth of field. AO-TPLSM with direct wavefront sensing can also counteract the intrinsic aberration of the GRIN lens by treating it as sample aberration with  $30\ \mu\text{m} \times 30\ \mu\text{m}$  isoplanatic patches<sup>32</sup>.

In addition to the improvement of imaging quality, the DM in the AO-TPLSM also serves as a convenient tool to manipulate the focus spot of the microscope. For example, the third Zernike mode of the DM, i.e., defocus, corresponding to Noll Index 4 (ref. 33), moves the focus along the optical axis without introducing extra aberration. With the fast settle time of the DM ( $\sim 0.5\ \text{ms}$ ), defocus can be used for multiplane imaging. The first two Zernike modes of the DM, i.e., tip, and tilt corresponding to Noll indices 2 and 3 (ref. 33), moves the focus along the  $X$  and  $Y$  axes, respectfully, and may be potentially used for online motion correction.

## Comparison with other methods

The essential task for AOs is the measurement of aberration to determine the phase map and program the DM to compensate for the optical aberration(s) (Fig. 1c,d). The direct wavefront sensing method we introduce provides reliable measurement of the aberrated wavefront for better SNR and greater imaging depth<sup>16</sup>. While the direct method is effective, indirect sensing methods have also been widely implemented in TPLSM<sup>19,26</sup> and even three-photon microscopy<sup>20,21,34</sup>. Instead of using a guidestar signal, the indirect methods infer the desired

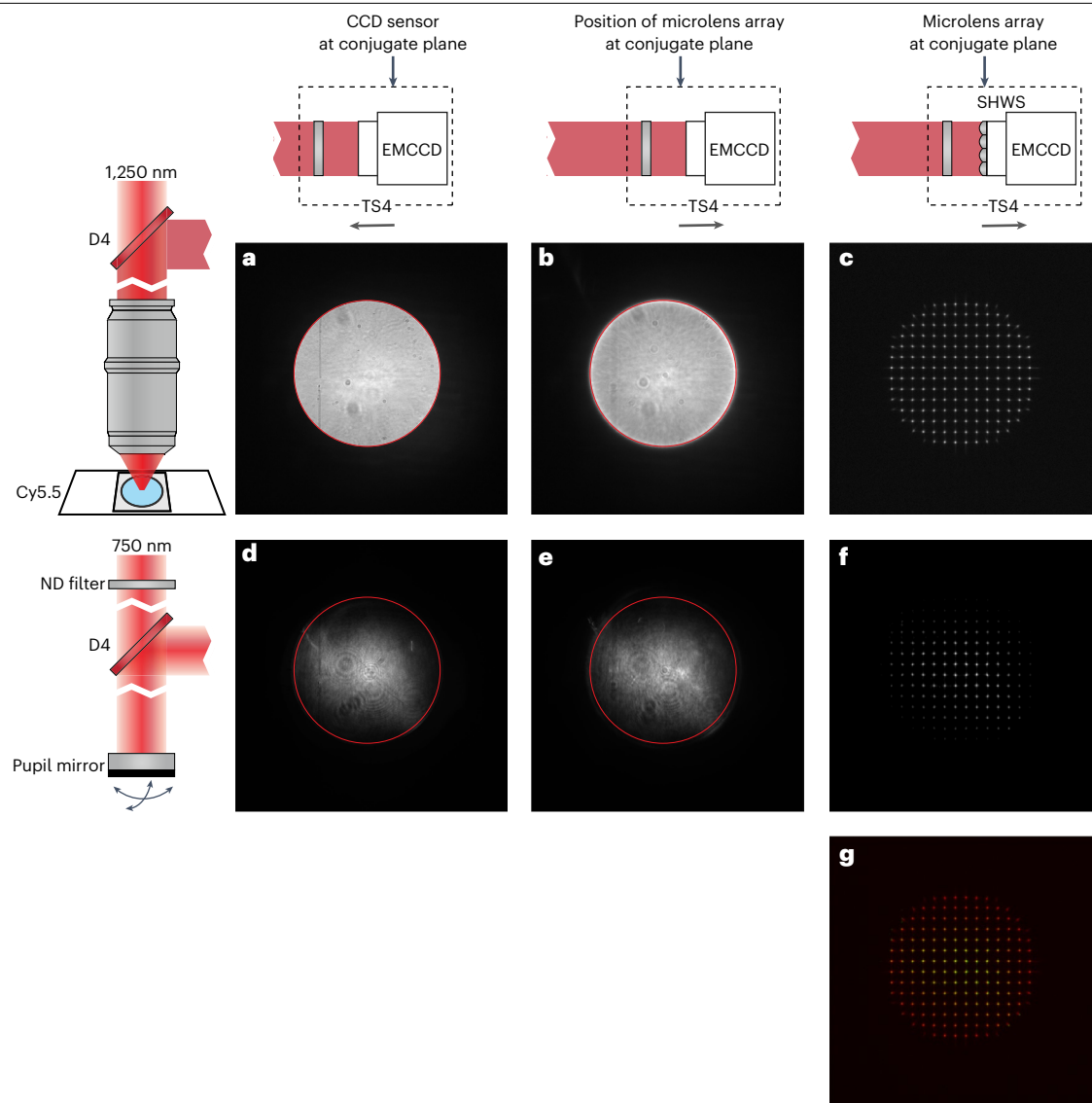


**Fig. 10 | AO calibration preparation.** The information in this figure relates to Steps 43–45. **a–f**, Images obtained on the EMCCD before the AO calibration. The diagrams on the left show the light source for the EMCCD images. Images in **a–c** were taken with the Cy5.5 fluorescence, and images in **d–f** used the femtosecond laser beam reflected by a mirror at the pupil plane. The diagrams at the top show the position of the EMCCD along the optical axis. Images in **a** and **d** were taken by the EMCCD at the conjugate plane (P1), images in **c** and **f** were taken by the

SHWS of which the microlens array is at the conjugate plane (P2), and images in **b** and **e** were taken with the EMCCD at the same position as **c** and **f** (P2) but no microlens array was placed on the light path. The edge of the bright disk in **a** was indicated by a red circle in images **a**, **b**, **d** and **e**, showing that the bright disks in the four images are concentric. **g**, Merge of **c** (red) and **f** (green). It is critical to the AO calibration that **a**, **b**, **d** and **e** are concentric, and that **c** and **f** are overlapped. Images in **c**, **f** and **g** have been gamma corrected to enhance visualization.

wavefront from the acquired images. Since the aberrated wavefront usually leads to a degraded image, one can find the desired wavefront by tuning it based on certain metrics of the image, such as the intensity. In general, indirect methods are easier to implement, as they do not have the wavefront sensing light path and no guidestar needs to be formed and measured, albeit they usually require more time than sensor-based direct methods as they utilize a collection of many images across multiple iterations. Among these indirect methods, we particularly highlight the Focus Scanning Holographic Aberration Probing method<sup>34,35</sup>. This approach effectively utilizes the properties of multiphoton absorption to measure and correct the distorted electric field point spread function in the sample without using guidestar. Notably,



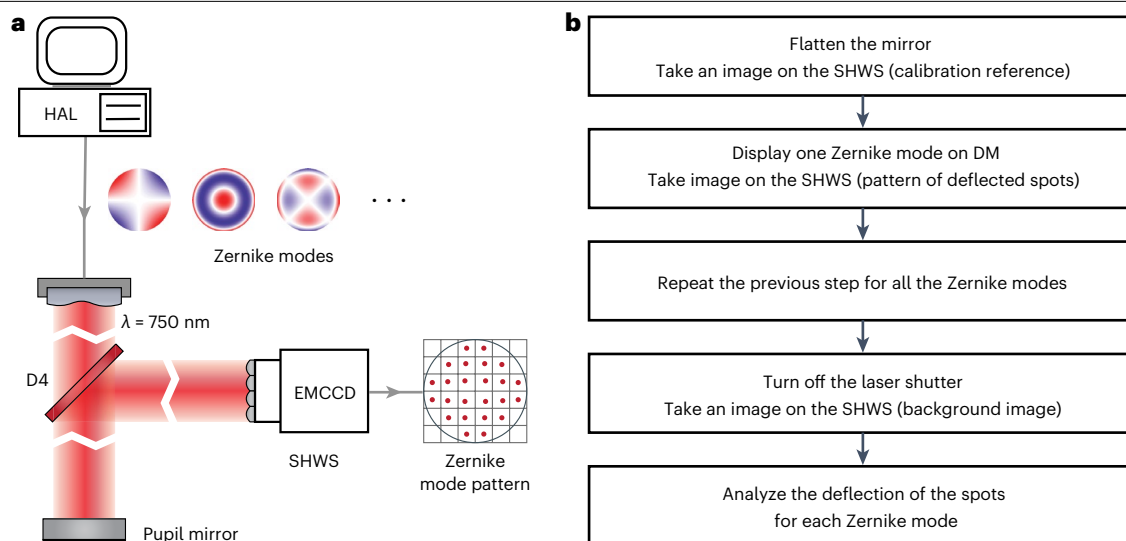


**Fig. 11 | AO calibration.** **a**, A schematic illustrating the AO calibration, relates to Steps 46–49. HAL, the computer for controlling the DM. **b**, Flowchart of the AO calibration procedure, corresponding to the MATLAB codes ‘DM\_SHWS\_calibration\_Ctr.m’ and ‘DM\_SHWS\_calibration.m’.

Focus Scanning Holographic Aberration Probing is capable of correcting both aberrations and scattering, making it well suited for imaging in scattering samples such as thinned-skull preparations.

Phase modulators are crucial components in AO systems as well. In addition to the continuous surface DM implemented in our system, SLMs are commonly used in microscopy<sup>19,26,34,35</sup>. SLMs enable precise phase modulation of wavefront segments by manipulating the refractive index of individual pixels. By altering the optical path length on a pixel-by-pixel basis, SLMs allow for the correction of more complex wavefront aberrations, and even for scattering. While it is theoretically possible to replace the DM in our system with an SLM, the primary limitation for more complex wavefront correction lies in accurately measuring the higher-order aberrations rather than the capabilities of the phase modulators. To effectively estimate higher-order aberrations, a larger number of deflected spots on the SHWS are required. However, this results in the guidestar signal being spread across multiple individual spots, leading to a reduction in the SNR of the image captured on the EMCCD during wavefront estimation. Furthermore, the DM has advantages over SLMs in certain aspects. The DM is not affected by chromatic effects, making it compatible for multiwavelength excitation. It also offers faster settling times compared with SLMs, which saves time during system aberration calibration. Nevertheless, it is still feasible to incorporate an additional SLM to the pupil plane alongside the DM, allowing for the flexibility to correct more complex aberrations when needed.

## Limitations

Limited by the scattering of the tissue, the maximum image depth of AO-TPLSM is ~900  $\mu\text{m}$  under the pia, where the guidestar pattern on the EMCCD degrades severely. The emission of Cy5.5 peaks at 703 nm; therefore, a guidestar with a longer emission wavelength is desired for improved deep wavefront sensing. Guidestars with longer emission wavelength also better represent the aberration of the excitation beam, which ranges from 800 to 1,300 nm.

Reducing the expansion ratio of the descanned guidestar can potentially increase the SNR of the image on the EMCCD by concentrating the light intensity on the microlens array. However, this will reduce the number of the focus spots for wavefront sensing and diminish the precision of the wavefront estimation.

The AO-TPLSM we described in this protocol is an open-loop system, which means that the wavefront sensor does not receive feedback about the actual wavefront after

# Protocol

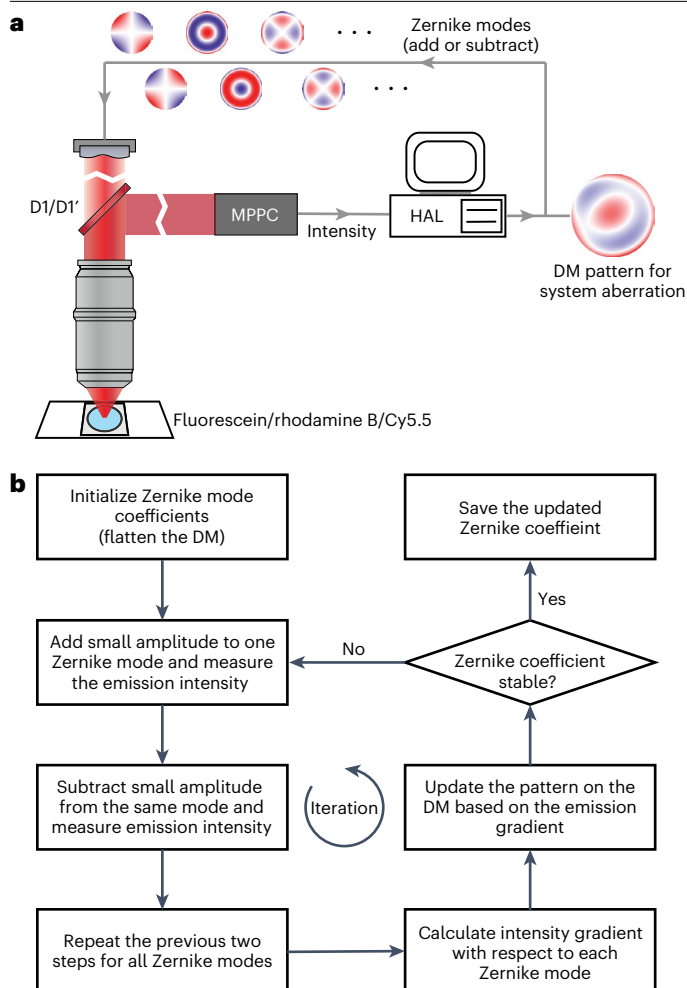


**Fig. 12 | Configuration for system aberration calibration. a,** A schematic illustrating the configuration for system aberration calibration, relates to Steps 50–51. HAL, the computer for controlling the DM. **b,** Flowchart of the system aberration calibration procedure, corresponding to the MATLAB codes ‘sensorlessWF\_sys\_abr\_descend.m’.

AO correction. This type of implementation is common in microscopy since the aberrations are mostly temporally static in biological samples. However, drift on the DM surface caused by temperature changes and mechanical creep can potentially degrade the correction performance in the open-loop system. In our experiments, we did not observe notable changes in the correction efficacy over hours. Nonetheless, to minimize the potential influence of the drift, we recommend purchasing the high-stability version of the DM optimized for open-loop systems and performing regular calibrations of the AO-TPLSM system.

We designed an entire AO-TPLSM system from scratch rather than modify an existing plan or commercial TPLSM system. This ensures ease of flexibility. We note that the bulk of the cost for the AO-TPLSM system are the AO components and a tunable 100-femtosecond laser.

## Expertise needed to implement the protocol

We designed the AO-TPLSM and detailed the construction steps to make it easy for laboratories with limited previous imaging expertise to setup, maintain and use the AO-TPLSM. Despite this, basic knowledge in optics, electronics and programming is required for the primary user, who is responsive for assembling, aligning and calibrating the system. Prior experience in constructing

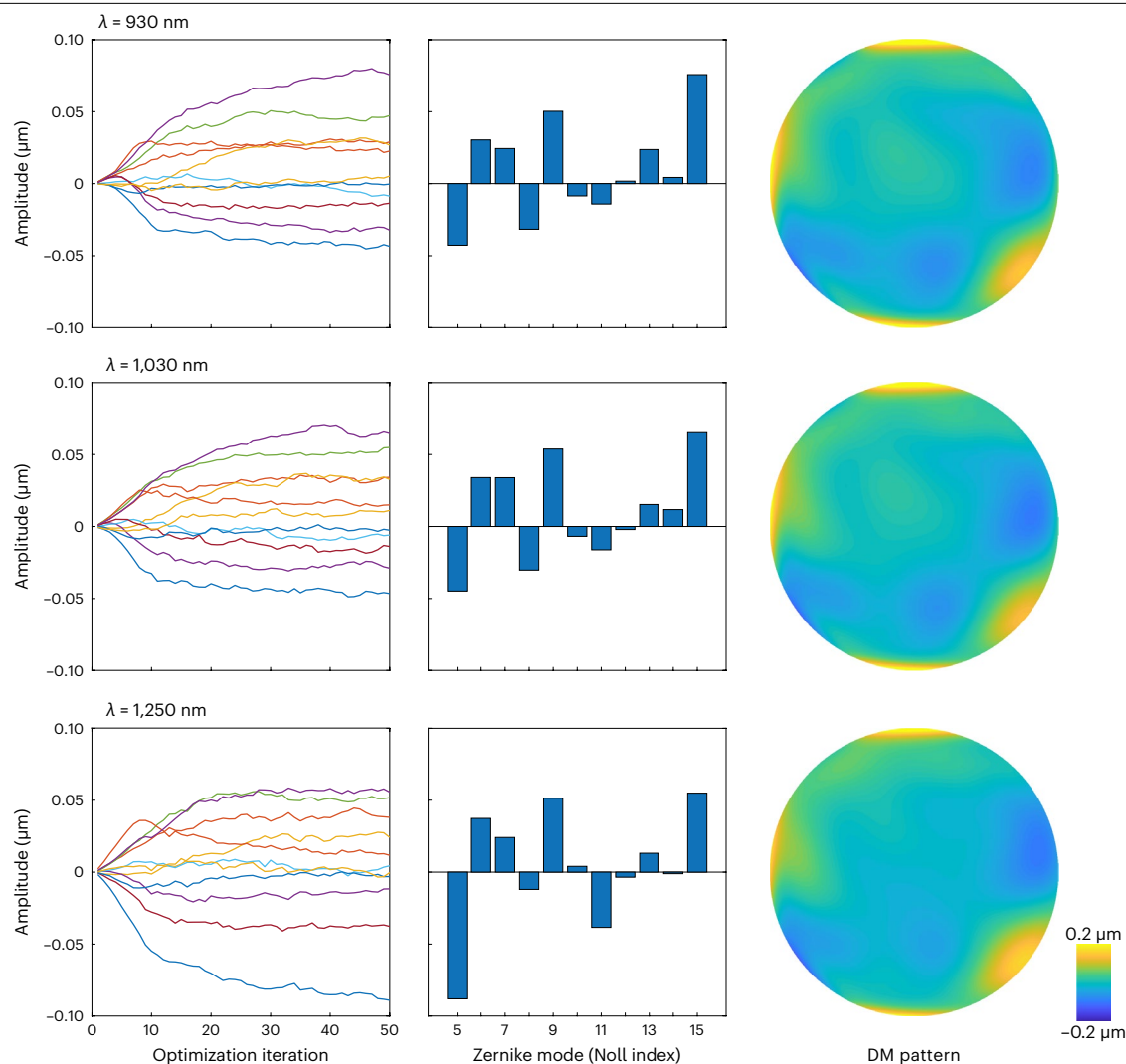


**Fig. 13 | Results for system aberration calibration.** Representative outcomes of system aberration calibration for the excitation beam in 930 nm (top), 1,030 nm (middle) and 1,250 nm (bottom), relates to Step 51. Left: the changes of Zernike coefficients as a function of optimization cycles. Middle: Zernike coefficients after 50 optimization cycles. Right: wavefront phase map on the DM that compensates for the system aberration.

imaging systems can facilitate the project but is not required. The users that are involved in the in vivo imaging experiment should have the ability to perform the craniotomy or thin-skull surgery and operate basic imaging software.

## Materials

### Equipment

- Optical table (at least 4' by 6' in extent, e.g., Newport, RS2000-56-12, 5' by 6' in extent)
- Tunable femtosecond laser (e.g., Coherent, Chameleon Discovery)
  - ▲ **CRITICAL** The wavelength of the laser must encompass 1,250 nm, at least 1,200 nm, with reasonable output power, i.e., at least 1,000 mW, for wavefront sensing with Cy5.5. The imaging depth that can be achieved by AO-TPLSM is largely determined by the maximum depth of wavefront sensing, which is constrained by the laser power.

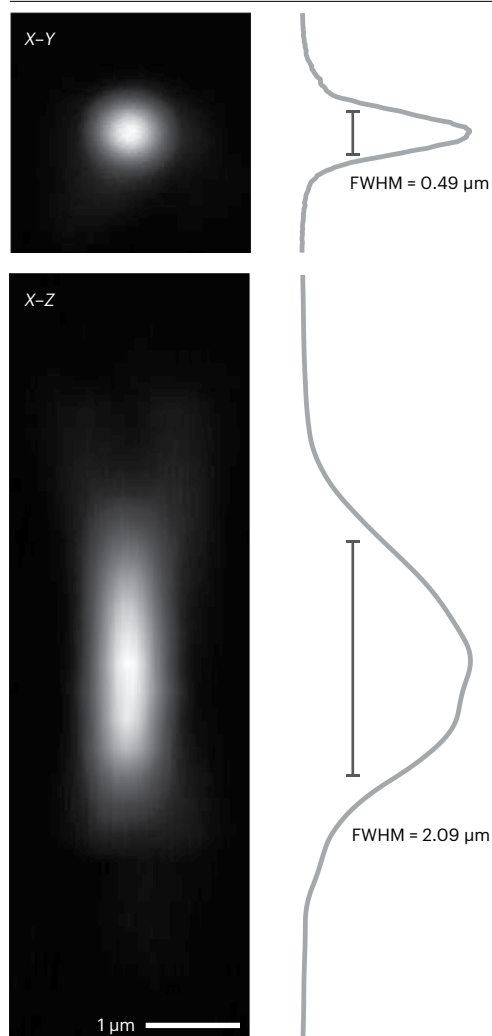


**Fig. 14 | Point spread function after system aberration correction.** Point spread function measured from a 200 nm diameter fluorescent bead after correcting the system aberration; relates to Step 52. Top: image of the *X*–*Y* plane with the signal profile showing the lateral resolution. Bottom: image of the *X*–*Z* plane with the signal profile, showing the axial resolution. FWHM, full width at half maximum.

The power efficiency of the AO-TPLSM at 1,250 nm is ~10–15% (power measured at the laser relative to power measured at the objective output). Previous studies reported that no photodamage was observed when using average incident laser powers of ~250 mW for in vivo imaging<sup>36,37</sup>. Therefore, ~2,000 mW of laser output at 1,250 nm should be ideal to generate 200–300 mW of excitation beam power for wavefront sensing without photodamaging.

- Optical components including the microlens array (Edmund, #64-483) (listed in Table 1)
- Optical electronics and opto-electronics including the DM (ALPAO, DM97-15) and EMCCD (Andor, DU-888U3-CS0-BV) (listed in Table 2)

▲ **CRITICAL** The trigger-option of the DM controller is required for synchronization between the DM and the ScanImage. We use the high-speed option of the DM97-15 in our implementation, which has quick settling time but less stroke (dynamic range) as the trade-off. The high-stability option should be more suitable for general users.

- Commercial opto-mechanics (listed in Table 3; the current price and link for the commercial parts in Tables 1–3 are provided in Supplementary Table 1)

# Protocol

- Custom opto-mechanics for AO-TPLSM are listed in Table 4 (the computer-aided design models and ancillary drawings for the customized parts are provided in Supplementary Data 2)
- Computer
  - ▲ **CRITICAL** The computer should have an extra PCI-e slot, ×1 or more, for the DM controller, besides meeting the requirement for the ScanImage PXI-based system ([https://archive.scanimage.org/SI2019/Supported-Microscope-Hardware\\_28377190.html#SupportedMicroscopeHardware-ComputerHardware](https://archive.scanimage.org/SI2019/Supported-Microscope-Hardware_28377190.html#SupportedMicroscopeHardware-ComputerHardware)).

## Software

- MATLAB (Version 2017b)
- NI DAQmx (Version 19.5.x)
- ScanImage (Version 2018b)
- ALPAO SDK (Version 3.08.08)
- Andor SOLIS
- Customized AO-TPLSM software (Supplementary Software)

## Reagents

The following fluorescent dyes are prepared as 0.2–0.5% (wt/vol) aqueous fluorescent solutions captured between a glass slide and a #1 cover slip for system aberration calibration.

- Fluorescein sodium salt (Sigma-Aldrich, cat. no. 46960)
- Sulforhodamine B (Invitrogen, cat. no. S1307)
- Sulfo-cyanine5.5 (sulfo-Cy5.5) (Lumiprobe, cat. no. 27320)

The following fluorescent beads are used for measuring the point spread function.

- 0.2 µm Yellow–green carboxylate-modified microspheres (Invitrogen, cat. no. F8811)
- 0.2 µm Red carboxylate-modified microspheres (Invitrogen, cat. no. F8810)

The following reagents are used to conjugate cyanine 5.5 to 2,000 kDa dextran as the in vivo fluorescent agent to form the guidestar.

- Cy5.5 *N*-hydroxysuccinimide (NHS) ester (Lumiprobe, cat. no. 27020)
- Amino-dextran 2,000 kDa (Finabio, cat. no. AD2000x250)
- Bicine (Sigma-Aldrich, cat. no. B3876)
- Econo-Pac chromatography columns (Bio-Rad, cat. no. 7321010)
- Dimethyl sulfoxide (DMSO), anhydrous (Thermo-Fisher, cat. no. D12345)
- *N*-succinimidyl-acetate (TCI Chemicals, cat. no. S0878)
- Spin columns 100,000 Da MWCO (Sartorius Vivaspin 6, cat. no. VS0641)

## Biological materials

- Wild-type mouse for thalamocortical bouton imaging. (C57BL/6J, Jackson labs, stock no. 000664)
- SST-tdTomato mouse generated by crossing SST-IRES-Cre mice (JAX, stock no. 013044) with Ai14 mice (Jackson labs, stock no. 007914).
- Rbp4-Cre mouse for layer 5 imaging. (MMRRC ID: 037128)
- AAV1.Syn.FLEX.NES-jRGECO1a.WPRE.SV40 (Addgene, cat. no. 100853-AAV1)
- AAV1.hSyn.FLEX.iGluSnFR3.v857.PDGFR (Addgene, cat. no. 175180-AAV1)
- Behavioral training for head fixation and surgical procedures to make cranial windows and to inject viruses were in accordance with best practices for the ethical treatment of laboratory animals. Our animal use protocol was approved by the Institutional Animal Care and Use Committee at the University of California San Diego.

## Equipment setup

A double-layer cover glass sample

1. Glue two number 1 cover glasses with optical adhesive (Norland optical adhesive 61).
2. Cut a 5 mm × 5 mm piece of Kimwipe, place it on a slide.

# Protocol

3. Add a drop of the 0.5% (wt/vol) sulforhodamine B (Invitrogen, S1307) and a drop of the 0.5% (wt/vol) sulfo-Cy5.5 (Lumiprobe, 27320) solutions, wait till the solutions dry, add a drop of instant adhesive (Loctite 4014) and close with the double-layer cover glass.

## Procedure

### Assembly of the AO-TPLSM with direct wavefront sensing

#### ● TIMING 5–10 d

▲ **CRITICAL** This section describes the assembly of the microscope (Steps 1–22), as shown in Fig. 4. Steps 1–16 describe the procedure to build a conventional two-photon microscope with a 4-f scanning system. Steps 17–19 and 20–21 emphasize the assembly for the DM module and SHWS module, respectively. Step 22 describes the wiring for the electronics. All the assembly drawings referenced in the instructions are provided in Supplementary Data 1. The system should be assembled in the order shown in the assembly drawings, denoted 'AD', and in Fig. 3a.

1. Mount the customized main breadboard (Thorlabs, PBG3048F, part drawing PD-01) onto the optical table (e.g., Newport, RS2000-56-12, 5' by 6' in extent), via four attached rails (Thorlabs, XT95-500 and XT95P3). Mount the center rail (Thorlabs, XT95-500 and XT95P3) vertically on the optical table as shown in assembly drawing AD-01.
2. Assemble the Z-motor unit (AD-02) and XY-sample stage (AD-03). Mount these components on the center rail and the optical table respectively, as shown in AD-04.
3. Assemble the lens pair L5 and L6, both of which consist of two achromatic doublets (Thorlabs, AC508-150-B), as shown in AD-05.
4. Insert the galvo scanner (Cambridge Technology, 6-mm 8315K X-galvo) and the resonant scanner (Cambridge Technology, CRS 8 kHz) into their holders (PD-05 and PD-07, respectively), as shown in AD-06 and AD-07. If a galvo-galvo scanning system is used instead of the resonant scanner, use the alternate holder (PD-05-backup) for the Y-galvo (Cambridge Technology, 6-mm 8315K Y-galvo).
5. Mount the lens pair L5 and L6, as well as the scanners, on the 4-f scanner module. Adjust the distance among each component as shown in AD-08.
6. Assemble the scan lens L7 (Newport, KPC070AR.16; Thorlabs, LB1199-B, and two of AC508-150-B; AD-09) and the tube lens L8 (Thorlabs, two of ACT508-500-B; AD-10). Mount these assemblies on the scan module, as shown in AD-11.
7. Mount the scanning module on the main breadboard, aligning the cutout hole on the custom vertical mounting plate (Thorlabs, CPVMP, PD-09) with the cutout hole on the main breadboard. Attach a mirror (M11, Thorlabs, PF10-03-P01) to the scanning module as the entrance for the excitation beam, as shown in AD-12.
8. Mount the microscope objective (Olympus, XLPLN25XSVMP2, 25×, 1.0 numerical aperture and 4 mm working distance) to the Z-motor via an objective mounting module (AD-13), as shown in AD-14.
9. Mount a 100-femtosecond pulsed laser with tunable wavelength, e.g., Coherent, Chameleon Discovery with a wavelength range of 680–1,300 nm, on the optical table. The main output port is followed by a shutter (Uniblitz, Shutter: LS6; Driver: VCM-D1), as shown in AD-15. Reserve the space on the optical table between the laser and the main breadboard as shown in AD-15, for a potential Pockels cell power control unit, the excitation beam expander and the periscope.
10. Depending on whether the laser has an internal laser power control, an external power control unit such as Pockels cell (ConOptics, Cell: 350-105-02; Driver: 302RM) may be required for modulation of the excitation power. Mount the Pockels cell on the optical table (ConOptics, Mount: 102A Adjustable Mount) and align with the laser output (AD-15).
11. Assemble a telescope, formed by a pair of plano-concave lenses (L1: Thorlabs, LA1805-B, AD-16; L2: Thorlabs, LA1484-B, AD-17), as shown in AD-18. This telescope is used to expand



the laser beam to fill, or slightly overfill, the aperture of the DM (ALPAO, DM75-15, pupil diameter: 13.5 mm).

▲ **CRITICAL STEP** The beam size varies according to the specific model of laser. Thus, the user should choose the L1 and L2 lens pair according to:

$$\frac{\text{Focal length}_{L2}}{\text{Focal length}_{L1}} = \frac{\text{Beam size}_{\text{out}}}{\text{Beam size}_{\text{in}}}$$

where the Beam size<sub>out</sub> represents the diameter of collimated beam output from telescope, which should match the pupil size of the deformable mirror, and the Beam size<sub>in</sub> represents the size of collimated beam input to the telescope, which could be approximated by diameter of the beam at the output of the power control. It is best to measure the beam diameter at the entrance of the beam expander with a beam profiler, e.g., Thorlabs, BP209IR1, and select the lens pair accordingly. For our specific realization, the beam is expanded tenfold by lens pair L1 and L2, which are chosen to have 30 and 300 mm focal lengths, respectively.

#### ◆ TROUBLESHOOTING

12. Mount a pair of mirrors, M1 and M2 (Thorlabs, PF10-03-P01), on the optical table followed by the telescope, as shown in AD-15. The mirror pair will be used for telescope alignment.
13. Assemble the periscope, formed by a pair of mirrors, M3 and M4, as shown in AD-19. Mount M4 on the edge of the main breadboard (AD-15) and mount M3 on the optical table vertically aligned with M4.
14. Assemble the emitted photon detection unit with the steps (AD-20) in Box 1.  
▲ **CRITICAL STEP** Keep some space between the aspheric lens and the filter, as shown in AD-20. Recall that the arrow on the edge of the bandpass filter indicates the direction for the light path. Block the unused thread hole with black room-temperature-vulcanizing (RTV) silicone cement (Momentive, RTV103) to prevent stray photons from leaking into the MPPCs.
15. Mount the dichroic filters to the customized dichroic mount (D1: Semrock, FF665-Di02-35×37-EB, AD-21; D1': Semrock, FF775-Di01-25×36, AD-22; D2: Semrock, FF552-Di02-25×36, AD-23; D3: FF662-FDi01-25×36, AD-23). Face the reflective coating side towards the midline of the dichroic mount; information about how to orient the dichroic filter is found at <https://www.idex-hs.com/contact/contact-us/faqs/optical-filters-faqs/what-is-filter-orientation>.
16. Assemble the acquisition module, consisting of lenses L11 (Thorlabs, LA1765-A, AD-24), L12 (Thorlabs, LA1027-A, AD-25), L13 and L14 (Thorlabs, LA1805-A, AD-26), as shown in AD-27. Mount the acquisition block to the Z-motor. Plug in the main dichroic (D1) and three MPPC modules, as shown in AD-28.  
▲ **CRITICAL STEP** Fill the corners and small gaps between the plates with black RTV cement to prevent stray photons from leaking to the MPPCs.
17. Assemble the DM translation stages (TS1 and TS2) on the main breadboard. Mount the DM (ALPAO, DM97-15) as well as a pair of mirrors M6 and M7 on the stage, as shown in AD-29.

## BOX 1

### Assembly of the emitted photon detection unit

1. Attach a custom mounting plate (LINOS Microbench, G061010000, PD-13) to the modified cover of MPPCs (three of Hamamatsu, C13366-3050GA, PD-12).
2. Affix an aspheric lens (L15: Thorlabs, A240-A) to the center hole of the MPPC cover with glue (Momentive, RTV103).
3. Insert the bandpass filter (Semrock, FF01-530/55-25 for the green/yellow channel, Semrock FF01-593/46-25 for the red channel or Semrock FF01-708/75-25 for the far-red channel) followed by a short pass filter (Semrock, FF01-790-SP-25) into the MPPC mounting plate.
4. Fix the position of the filters with set screws.

Depending on the placement of the periscope, one extra mirror (M5) may be required to feed the excitation beam from the periscope to the DM module.

▲ **CRITICAL STEP** To minimize the alignment effort when moving the TS1 (Step 38), mirrors M5 and M6 should be located such that the beam between M5 and M6 is near parallel to the direction of travel of TS1. Similarly, locate mirrors M6 and M7 such that the beam is parallel to the direction of travel of TS2. To avoid mirror M7 blocking the reflected light from deformable mirror, a small incident angle, i.e.,  $<5^\circ$ , is introduced at the DM by adjusting the position of mirror M7 on the stage TS2 (Fig. 3a; AD-29).

18. Mount lens L3 (Newport, KPX117AR.18,  $f=450$  mm, AD-31) on the main breadboard and attach L4 (Newport, KPX100AR.18,  $f=150$  mm, AD-32) to the 4-f scanner module (AD-33), as shown in AD-30. Lens pair L3 and L4 form a telescope that demagnifies the beam, threefold, from the DM to fit the aperture of the scan mirrors.
19. Mount a mirror M8 followed by a translation stage (TS3) for the mirror pair M9 and M10 (Thorlabs, PF10-03-P01, AD-34) on the main breadboard. These are used for fine adjustment of the optical path between lenses L3 and L4, as shown in AD-30.

▲ **CRITICAL STEP** To minimize the alignment effort, the mirror pair M9 and M10 should be placed so that the beam between M10 on the TS3 and M11 in the scanning module is about parallel to the direction of travel of TS3. One means to achieve this is to temporarily link the M10 and M11 mirror mounts with long rods and locate the position for the M9 and M10 mirror pair before mounting them on the TS3. Similarly, place M8 in a way such that the incident beam to the M9 travels parallel to the direction of travel of TS3.
20. Attach a dichroic (D4: Semrock, FF775-Di01-25×36, AD-35) to the scanning module followed by a 4-f relay for wavefront sensing (AD-36), formed by a pair of achromatic doublet lenses (L9: Thorlabs, AC254-125-A,  $f=125$  mm, and L10: Thorlabs, AC254-200-A,  $f=200$  mm) and a pair of reflective mirrors (M12 and M13), as shown in AD-38.
21. Mount the SHWS module, consisting of an EMCCD (Andor, iXon Ultra 888) and a microlens array (Edmund, #64-483), on the main breadboard via a translation stage (TS4), as shown in AD-37 and AD-38.
22. Connect the electronics and setup the computer data file for the ScanImage; information about wiring and machine data file for the ScanImage PXI-based system is found at <https://archive.scanimage.org/SI2019/28377185.html>.

▲ **CRITICAL STEP** The frame clock of ScanImage (Primary DAQ, Port: PFI6) will be used as the trigger signal for the deformable mirror. A NOT-gate is required since the PCI-E interface of the DM controller (PEX-292144) supports trigger on falling edge only.

## Alignment for the AO-TPLSM

### ● TIMING 10–15 d

▲ **CRITICAL** This section describes the alignment for process for the microscope (Steps 23–42). Steps 23–37 describe the basic alignment for the microscope while Steps 38 and 39–41 emphasize the fine adjustment on the excitation path and direct wavefront sensing path, respectively, to conjugate scanners, DM and SHWS to the pupil plane of the objective. For the basic alignment and the DM conjugation (Steps 23–36 and 38), we recommend tuning the laser to the most used wavelength for your application, e.g., 930 nm for excitation of GCaMP, and visualize the beam with an infrared (IR) viewer (e.g., Newport, IRV2-1300). An IR detector card (e.g., Thorlabs, VRC4) is handy to localize the beam during alignment. The laser power can be modulated by applying a voltage to the crystal in the Pockels cell. However, prolonged exposure to high voltage can cause the crystal to decay. To avoid this, we recommend using a low output power, e.g., ~100 mW, during the alignment. This power level does not require excessive voltage on the crystal, while still being strong enough to be visualized by the IR viewer.

▲ **CAUTION** Always follow the laser safety protocol when using the laser. Appropriate laser safety eyewear is always required during the following procedure.

▲ **CAUTION** It is crucial to emphasize that even at this power level, the laser beam can still cause severe eye damage if it accidentally enters the eye. Therefore, it is absolutely essential to wear appropriate laser safety eyewear during the alignment process.

23. Open ScanImage. Click the 'Direct Mode' checkbox and adjust the power on the Power Controls Panel. Click the 'Point' button on the Main Controls Panel. Flatten the DM by clicking the 'Flatten DM' button on the AO control panel, labeled as 'AOGUI'.  
**▲ CRITICAL STEP** After starting the ScanImage, the scanners will be oriented towards the park angles, as set in the machine data file. Clicking the 'Point' button will bring them back to zero degrees and open the shutter for the alignment; information about the 'Point' button is at [https://archive.scanImage.org/SI2019/Main-Controls\\_28377140.html](https://archive.scanImage.org/SI2019/Main-Controls_28377140.html).
24. Align the laser output with the center of the beam expander. An alignment plate with a pinhole (Thorlabs, CPA1) can be used to indicate the center of the beam expander. Adjust the positioning knobs on mirrors M1 and M2 so that the beam is centered at the pinhole on the alignment plate while moving the plate back and forth along the rail to check for parallel alignment.  
**▲ CRITICAL STEP** We recommend temporarily removing lenses L1 and L2 from the cage system during the alignment to make the beam path more intuitive.
25. Adjust the distance between lenses L2 and L1 to collimate the output from the beam expander (Fig. 6a).  
**▲ CRITICAL STEP** Introduce a temporary mirror after the telescope to project the expanded beam to a distant location and visualize the beam by the IR detector card. You should not see notable changes in beam size along the beam path if the beam is well collimated. If the beam size increases along the projection, you should move lens L2 away from L1 along the cage system, and vice versa.  
**◆ TROUBLESHOOTING**
26. Adjust the directions of mirrors M3 and M4 to align the beam to the center of the periscope cage system, as indicated by the iris (Thorlabs, CP20D) that moves along the rail.
27. Adjust the orientation of mirrors M5, M6 and M7 to align the periscope output beam to the deformable mirror. Tune the orientation of the DM rotation stage (Thorlabs, PR01) and TS2 to align the DM output beam to the lens L3 cage system. The alignment of DM in axial direction will be introduced in Step 38.  
**▲ CRITICAL STEP** As for Step 24, we recommend temporarily removing lens L3 from the cage system and use the alignment plate (Thorlabs, CPA1). Ensure that the beam is not blocked by M7, as discussed in Step 17.
28. Adjust the distance between the DM and lens L3 to be ~450 mm by moving lens L3 along the cage rails.
29. Align the incident beam to the M9 mirror by tuning the direction the beam reflecting from mirror M8.  
**▲ CRITICAL STEP** As we discussed in Step 19, the ideal direction of the incident beam to the M9 mirror should be parallel to the direction of travel of TS3. Place an iris in front of the M9 mirror via temporary rods and adjust M8 until the beam stays on the center of the iris while the iris is moved along the rods.
30. Orient mirrors M9 and M10 to align the reflective beam to the center of iris (Thorlabs, CP20S) sliding along the rods at the entrance of the scanning module.
31. Tune the orientation of mirror M11 to make the beam go up vertically at the center of the cage system. You may wish to temporarily remove the X-galvo, as well as the caps on the X-galvo cube, and mount an iris (e.g., Thorlabs, SM2D25D) on the top of the cube via rods for the alignment procedure.  
**▲ CRITICAL STEP** The dichroic mirror (D4), whose function is to reflect the emission light coming back from the sample to the SHWS, may slightly shift the excitation beam in this section of the beam path. We recommend you adjust the dichroic approximately toward the same direction as we shown in AD-38 during the alignment in this step. This will minimize the influence on the excitation path while aligning the SHWS path in Step 39.
32. Rotate the galvo holder in the mount plate to align the excitation beam to the center of the 4-f cage system indicated by an alignment plate (Thorlabs, LCPA1) sliding along the rail.  
**▲ CRITICAL STEP** We recommend you take lens pair L5 and L6 off from the cage system for the initial alignment. Without L5 and L6, this segment of beam path could also be used to check the collimation of the output from the beam compressor lens pair L3 and L4. Reduce

the optical path between the L3 and L4 by moving the M9–M10 module along the rail if you find that the beam shrinks as it travels between the two scanners, and vice versa.

▲ **CRITICAL STEP** After you restore the lens pair L5 and L6, check whether the beam remains at the center of the cage system. If not, tune the L5 and L6 translation mounts (Thorlabs, CXY2) to bring the beam back to the center of the cage system and the center of the resonant scanner, respectively.

33. Rotate the resonant scanner in the holder to align the beam to the center of the cage system between the scanner and the folding mirror.

▲ **CRITICAL STEP** We recommend you remove scan lens L7 for the initial alignment and tune the position of the translation mounts (Thorlabs, CXY2) of the lens tube to recenter the beam as needed.

34. Adjust the folding mirror (Thorlabs, PFE20-P01, Mount: KCB2EC) and the tube lens (L8) translation mounts (Thorlabs, CXY2) to align the beam to the center of lens L8.

▲ **CRITICAL STEP** Mount an iris (Thorlabs, SM2D25D) on the L8 lens tube temporarily to assist with the alignment.

35. Align the beam to the back (pupil).

▲ **CRITICAL STEP** We recommend replacing the objective with an iris (Thorlabs, CP20S) that is mounted at the pupil plane (AD-39), as shown in Fig. 7b. Adjust the nonaxial position of the back aperture by sliding the objective module along the rail and changing the position of the Z-motor (Thorlabs, LNR502) horizontally on its mount (Thorlabs, XT95RC4). This step aligned the location of the back pupil in *x*–*y* direction, its alignment in axial direction will be introduced in Step 36. You can check this alignment using the EMCCD, as discussed later in Steps 43–44.

36. Check the conjugation between the scanners and the back aperture of the objective (Fig. 7a). Ideally, the X-scanner, Y-scanner and the back focal plane are conjugate, following the dimensions in the assembly drawing (AD-05, AD-08, AD-09, AD-10, AD-11, AD-14). However, we recommend that users verify the conjugation by observing the bright ring on the iris at the pupil level, indicated by the white arrow in Fig. 7b, while scanning. You should observe no movement of the bright ring if the scanners and back focal plane are well conjugated. If you observe movement, translate the pupil along the axial direction by the Z-motor to the level where you see no movement of the spot during scanning. This step confirms the location of the back pupil in axial direction, its alignment in *x*–*y* direction was introduced in Step 35.

37. Align the collection path. Adjust the main dichroic mirror (D1 or D1') to maximize the image brightness while imaging the sulfo-Cy5.5 solution (excitation beam: 1,250 nm) with the far-red channel. Similarly, adjust D2 and D3 while imaging the fluorescein solution (excitation wavelength: 930 nm) and the sulforhodamine B solution (excitation wavelength: 1,030 nm) through the green–yellow channel and red channel, respectively.

38. Conjugate the DM to the back focal plane of the objective.

▲ **CRITICAL STEP** To find the conjugate plane for the DM, temporarily replace the DM by a scratched mirror (AD-41) and image it by a camera whose sensor is at the objective back focal plane (AD-40). Slide stage TS1 until the camera obtains the clear and sharp image of the scratched mirror, as shown in Fig. 8. Put the DM back after you find the conjugate plane and adjust the alignment if necessary.

39. Excite the sulfo-Cy5.5 solution with the 1,250 nm excitation beam and align the emission beam to the wavefront sensing path from dichroic mirror D4 to L10 by tuning the orientation of dichroic D4 and mirrors M12 and M13.

▲ **CRITICAL STEP** Mount a camera, the same one you used for the DM conjugation, in the cage system for the initial alignment if you find the emission light too dim to be visualized by the IR viewer or an IR card.

▲ **CRITICAL STEP** Use dichroic mirror D1, and not D1', as the main dichroic so that most of the emitted light will go to the wavefront sensing path rather than the collection path.

40. Temporarily remove the microlens array from the SHWS. Open the Andor SOLIS software. Adjust the lateral and vertical position of the EMCCD to locate the emission beam at the center of the EMCCD. Adjust mirrors M12 and M13 until the beam position on the EMCCD stays fixed as the stage TS4 travels along the axial direction (Fig. 10a,b). Adjust the

distance between lens pair L9 and L10 until the beam size does not change as the EMCCD travels axially.

▲ **CAUTION** Always keep the short pass filter (Semrock, FF01-790-SP-25) in front of the highly sensitive EMCCD to protect it from scattered light from the excitation laser.

41. Mount the microlens array back in the SHWS and slide it along the rail until it focuses the emission light on the EMCCD.

▲ **CRITICAL STEP** Mount a stopper on the rail (Thorlabs, ERCPS) to mark the relative position for the microlens array, as the array will be removed and replaced several times for testing of conjugation and for calibration. Measure and calculate the distance between to lens array and the EMCCD sensor (AD-37), marked as Dist1.

42. Find the plane that conjugates to the objective back focal plane on the SHWS path.

▲ **CRITICAL STEP** Mount a paper target at the level of the objective back focal plane (AD-42) and illuminate it with a flashlight, with the laser off, as shown in Fig. 9. Remove the microlens array and move the EMCCD axially to the conjugate plane, where it obtains the sharp image of the paper target. Read the micrometer on stage TS4 and mark this position as P1. Restore the lens array and move stage TS4 axially for Dist1 to bring the lens array to the conjugate plane (marked as P2).

## AO calibration

### ● TIMING 2–5 d

▲ **CRITICAL** This section describes the calibration of the AO-TPLSM system (Steps 43–49). The purpose for the AO calibration is to map the phase shifts for each Zernike mode at 1  $\mu\text{m}$  root-mean-square (RMS) amplitude on the DM to the spot shifts on the SHWS, which will be used to calibrate and calculate the command signals to the DM module to correct for sample aberration.

43. Map the DM to the field of the SHWS (Box 2).

▲ **CAUTION** Always double check the positioning of the neutral density (ND) filter for the steps that directly reflect the laser to the EMCCD.

### ◆ TROUBLESHOOTING

44. It is critical for the AO calibration to map the DM and the objective back aperture at the same location on the SHWS (Box 3).

45. Set up the system in the same manner as in Step 43. Move the EMCCD to P2 and tune the direction of the pupil mirror to fit the calibration beam into the edge you have drawn at P1, as shown in Fig. 10e. Remount the microlens array. Finely tune the pupil mirror to overlap the current pattern on the EMCCD (calibration reference pattern, Fig. 10f) to the sample reference pattern as much as possible (Fig. 10g).

▲ **CRITICAL** The mismatch of the calibration reference pattern with the sample reference pattern will reduce the dynamic range for wavefront sensing.

### ◆ TROUBLESHOOTING

## BOX 2

### Steps to map the DM to the field of the SHWS

1. Remove the microlens array from the SHWS, keeping the short pass filter, and move the EMCCD to P1.
2. Replace the objective by a mirror mounted at the back focal plane (AD-43).
3. Mount an ND filter at the end of the lens pair L1 and L2 beam expander (e.g., Thorlabs, ND30A, Optical Density: 3.0) to protect the EMCCD by reducing the laser power.
4. Flatten the DM.
5. Tune the laser wavelength to 740–750 nm.
6. The calibration beam incident on the DM will be reflected by the pupil mirror and project to the EMCCD, where the DM will be seen as a bright disk with a sharp edge in the SOLIS software after adjusting the contrast and brightness, as shown in Fig. 10d. The sharp edge of the bright disk is the edge of the DM because the DM is conjugated to the EMCCD in this setting.
7. Use the region of interest (ROI) tool in SOLIS to draw a circle on the edge of the DM.



## BOX 3

### Steps to map the DM and the objective back aperture at the same location on the SHWS

1. Temporarily remove the lens array and keep the EMCCD at P1. Remove the ND filter and put the objective back in the system.
  2. Excite the sulfo-Cy5.5 solution with the 1,250 nm excitation beam, as shown in Fig. 10a. The emission light collected by the objective will appear as a disk with a sharp edge (back aperture disk) in the SOLIS software.
  3. Adjust the objective mounting module nonaxially until the back aperture disk is concentric with the DM edge, as shown in Fig. 10a,d.
  4. Double check the alignment after the adjustment by moving the EMCCD to P2 to confirm whether the beam position on the EMCCD remains motionless (Fig. 10a,b). If not, adjust the system as described in Step 40.
  5. Replace the microlens array and obtain an image with the SOLIS software as a sample reference pattern (Fig. 10c).
- 
46. Close the SOLIS software to release control of the EMCCD and initialize the DM and SHWS from MATLAB by clicking 'initialize DM' and 'initialize SH' bottom on the AOGUI. Click 'Camera config' to set the temperature as  $-60^{\circ}\text{C}$  for the EMCCD and turn on the chiller.  
▲ **CRITICAL STEP** Acquire images before the calibration to find a laser power and exposure time for clear images after the EMCCD reaches its target temperature.
  47. Run the first section of the code 'DM\_SHWS\_calibration\_Ctr.m', which will display each of the 60 individual Zernike modes on the DM and acquire an image of the deflected spots on the SHWS (Fig. 11). The code will also download a flat pattern to the DM to acquire a wavefront spot pattern for calibration reference. After the first section of the code is complete, turn off the shutter and run the second section of 'DM\_SHWS\_calibration\_Ctr.m' to obtain a background image. Save 'DM\_calibration\_shdata', 'DM\_calibration\_shdata\_ref' and 'DM\_calibration\_shdata\_ref\_bg' for the analysis in next step.
  48. Run 'DM\_SHWS\_calibration.m', which will analyze the deflection of the spots on the SHWS relative to the calibration reference for each Zernike mode. This part of the code will show the putative pattern of the DM versus the ideal Zernike modes. The putative pattern should look like the ideal one, except that it may be rotated or inverted.  
▲ **CRITICAL STEP** Before running the code, adjust the parameter for the center and the radius of the field-of-view (FOV) (lines 65–67) based on the back aperture disk on EMCCD, as previously obtained in Step 44.  
◆ **TROUBLESHOOTING**
  49. Click 'Camera config' to set the temperature as  $20^{\circ}\text{C}$  for the EMCCD and release control of the EMCCD from MATLAB by clicking 'deinitialize SH' after it reaches  $20^{\circ}\text{C}$ . The temperature of the EMCCD can be checked by clicking 'check temp'.  
▲ **CAUTION** Always use the temperature control to return EMCCD back to the room temperature ( $20^{\circ}\text{C}$ ) before turning it off.

### System aberration calibration

#### ● TIMING 2–3 h

▲ **CRITICAL** The purpose for the system aberration calibration is to find a pattern on the DM that compensates for the aberration introduced by the imaging system itself, which includes the imperfections of the microscope as well as aberrations induced by the cover glass of the cranial window (Steps 50–52). We suggest the system aberration should be corrected for all the wavelengths that are commonly used during experiments, as some components of the aberration, e.g., spherical aberration, vary with the wavelength (Fig. 13). We recommend



the use of aqueous solutions of the fluorescent dyes fluorescein, sulforhodamine B, and sulfo-Cy5.5 to correct the system aberration for 930, 1,030 and 1,250 nm excitation, respectively.

50. Flatten the DM by clicking the 'Flatten DM' button on the AOGUI. Image the central  $100\ \mu\text{m} \times 100\ \mu\text{m}$  field of the fluorescent sample at the depth of  $50\ \mu\text{m}$  under the cover glass (thickness number 1).  
**▲ CRITICAL STEP** Use dichroic mirror D1 as the main dichroic for fluorescein and sulforhodamine B imaging and use the D1' for sulfo-Cy5.5 imaging.
51. Run 'sensorlessWF\_sys\_abr\_descend.m' to implement a gradient-descent algorithm that optimizes the amplitude of each Zernike mode to maximize the average intensity (Fig. 12). In each iteration, the increments of the Zernike mode coefficients are computed based on the gradient of mean intensity changes to update the pattern on the DM. Tip, tilt and defocus are excluded. The coefficients of the Zernike modes usually became stable after 30–50 cycles of optimization (Fig. 13); you can set the number of iterations at line 18 of the code. The resulting Zernike coefficients will be referred as system aberration correction coefficients.
52. Validate the system aberration correction coefficients by measuring the point spread function of the 200 nm fluorescent beads after loading the system aberration correction pattern on the DM (Fig. 14).
53. Image the aqueous solution of sulfo-Cy5.5 after system aberration correction (main dichroic: D1',  $100\ \mu\text{m} \times 100\ \mu\text{m}$  field,  $50\ \mu\text{m}$  under the cover glass). Switch the main dichroic to D1 to obtain a sample reference pattern on the SHWS that will be used for sample aberration correction.

## System verification

### ● TIMING 2–3 h

**▲ CRITICAL** Improper calibration is a common cause for poor performance with AO in actual experiments. It can even lead to image degradation after aberration correction. To avoid this problem, we recommend evaluating the performance of the AO-TPLSM system on a fiber test sample.

54. Start ScanImage. Turn on the EMCCD and SOLIS software. Set the charge-coupled device temperature to  $-60\ ^\circ\text{C}$ .
55. Initialize the DM and flatten it. Acquire a  $50\ \mu\text{m} \times 50\ \mu\text{m}$  FOV image of a branch of a fiber (Fig. 15a).
56. Load the system aberration correction coefficients for acquisition at 1,030 nm to the DM.
57. Acquire an image for the same branch of the fiber with the same laser power as Step 55 (Fig. 15b).
58. Use dichroic mirror D1' as the main dichroic. Tune the laser to 1,250 nm for Cy5.5 and load the system aberration correction coefficients for acquisition at 1,250 nm.
59. Image the same FOV as in Step 57 with the far-red channel to confirm the existence of Cy5.5 in the FOV.
60. Replace dichroic mirror D1' with mirror D1 to transmit the far-red emission light of Cy5.5 to the wavefront sensing path.
61. Obtain the sample aberration pattern on the SHWS with the SOLIS software by a long exposure, i.e., 0.5 s, during scanning.
62. Save the sample aberration pattern (Fig. 15c). Run 'sample aberration correction' to compute the coefficients for sample aberration correction (Fig. 15d). The spherical aberration (Noll index 11 (ref. 33)) should dominate the correction pattern for the double-layer cover glass in a well calibrated system (Fig. 15e).
63. Add the sample aberration correction coefficients to the system aberration correction coefficients for 1,030 nm and send it to the DM.
64. Acquire an image for the fiber using the same FOV and same power, as in Steps 55 and 57 (Fig. 15f).
65. Compare the three images. A good calibration should give you about a two-fold increase in the intensity and a concomitant increase in SNR at this setting (Fig. 15g).

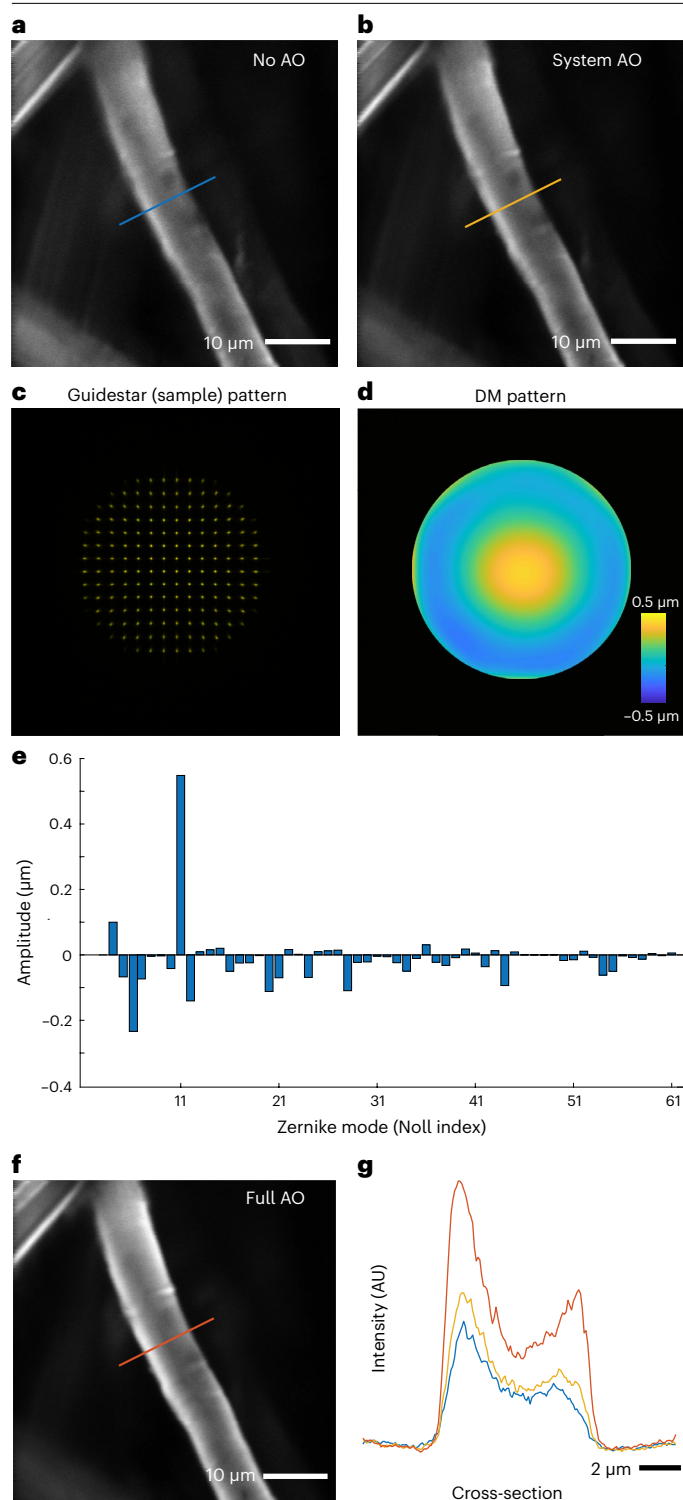


**Fig. 15 | System verification by correcting the aberration of the double-layer cover glass.** The information in this figure relates to Steps 54–65. **a, b**, Images of a fiber stained with rhodamine B, without any AO correction (**a**) and after correcting the system aberration (**b**). **c**, Spot patterns formed by the SHWS from the descanned guidestar signal for inferring the sample aberration. **d**, Reconstructed wavefront that applied to the DM. **e**, Zernike coefficients of the reconstructed wavefront. **f**, Image of the same object in **a** and **b** taken with both system aberration and sample aberration corrected. **g**, Signal profiles along the lines in **a, b**, and **f**.

# Protocol

## Synthesis of guidestar (2,000 kDa Cy5.5–dextran)

### ● TIMING 2 d

66. Prepare 50 mM bicine buffer at pH 8.5, adjust with NaOH. Store at 4 °C.
67. Dissolve 166.3 mg of amino dextran in 1,040  $\mu$ L bicine buffer. Add up to an extra 200  $\mu$ L buffer if it does not dissolve well as the solution is close to the saturation limit. Use a 50 mL Falcon tube for this process.
68. Dissolve 5 mg Cy5.5 NHS ester in anhydrous DMSO by adding 650  $\mu$ L of DMSO to the 5 mg Cy5.5 NHS ester in the Falcon tube. Gently swirl and then centrifuge down for 30 s.  
**▲ CAUTION** This solution is unstable and should be used immediately after preparation.
69. Mix dextran and Cy5.5 NHS ester, vortex and incubate for 2 h at room temperature. The solution should get a little warm from the reaction.
70. Dissolve 30.7 mg of *N*-succinimidyl-acetate (quencher) in 130  $\mu$ L of anhydrous DMSO in a 1.5 mL tube.  
**▲ CAUTION** This solution is unstable and should be used immediately after preparation. *N*-succinimidyl-acetate reacts with H<sub>2</sub>O, so always store *N*-succinimidyl-acetate in N<sub>2</sub> and work quickly after opening.
71. Add *N*-succinimidyl-acetate solution to the reaction and incubate overnight at 4 °C.
72. Suspend Sephadex G25 (in the separation column box) in PBS pH 7.4; for one batch use either 2 or 3 g Sephadex and add PBS to reach 50 mL. Allow some time to equilibrate, e.g., overnight at 4 °C.
73. Decant the PBS to leave 5 mL PBS on top of the Sephadex, vortex, and add to chromatography columns; wait for the Sephadex to compact and add the top frit. Slowly push it down until it just touches the Sephadex. Pour off the remaining top layer of PBS and equilibrate the column with 10 mL fresh PBS.  
**▲ CAUTION** Never let the Sephadex column run dry, or it will need to be discarded.
74. Add 2–3 mL of PBS pH 7.4 to the reaction mixture and load onto the Sephadex chromatography column.
75. Wait for the dye to completely enter the Sephadex.
76. Add some PBS, i.e., fill the column, and collect 'blue' fraction from the column into a 50 mL Falcon tube. Stop collecting when the bottom of the column becomes transparent.
77. Load 'blue' fraction into spin column(s) and centrifuge for 4 h at 4 °C at 4,000g (swinging bucket rotor) or 5,000g (fixed rotor).

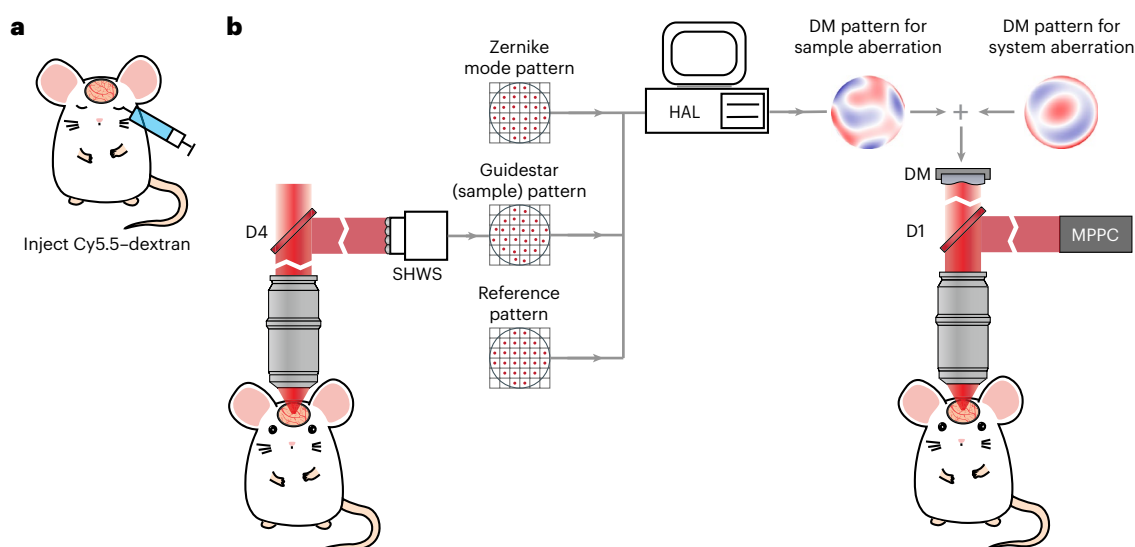


**Fig. 16 | In vivo experiment workflow.** The information in this figure relates to Steps 79–85. **a**, A schematic of the guidestar (Cy5.5–dextran) delivery by retro-orbital injection. **b**, A schematic diagram of the AO correction. Spot patterns formed by the SHWS from the descanned guidestar signal in the capillary,

together with the sample reference pattern and AO calibration results of the DM Zernike modes, are used for calculating the DM pattern for correcting the sample aberration. The sample aberration correction pattern is added to the system aberration pattern for full AO correction.

# Protocol

78. Collect the supernatant, which is Cy5.5-dextran; dilute it to 5 mL with saline, sterile filter and store at  $-20^{\circ}\text{C}$ .

## AO-TPLSM imaging with microvessels-based guidestar

### ● TIMING 1 d

▲ **CRITICAL** This section (Steps 79–85) describes the process (Fig. 16) to imaging structure (Fig. 17) and function (Fig. 18) of the mouse brain with AO-TPLSM. The animals should be prepared in the same manner as for conventional TPLSM, including the viral injection, craniotomy, or other special

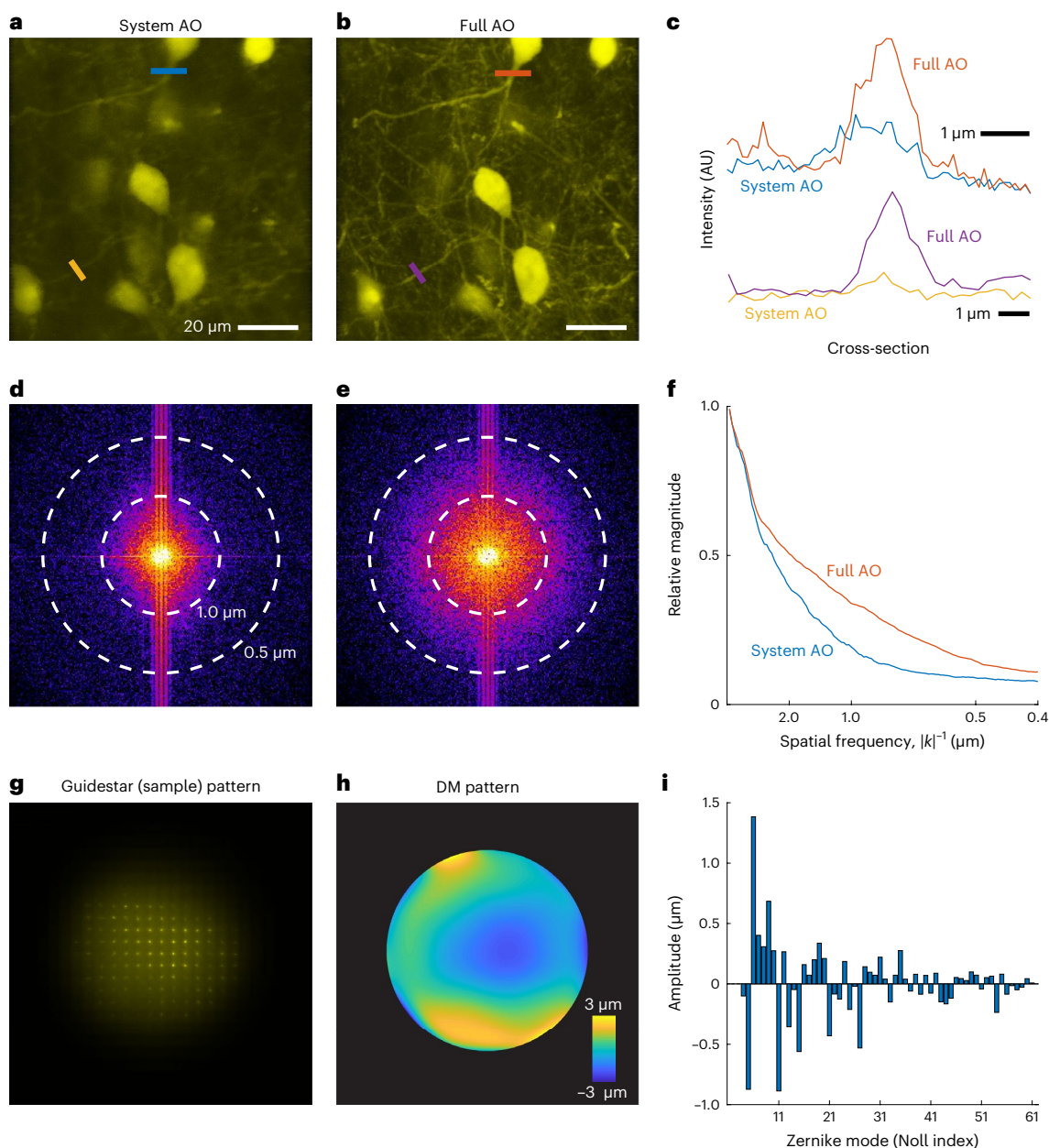


**Fig. 17 | Morphological imaging with AO correction.** **a,b**, SST<sup>+</sup> neurons in mouse somatosensory cortex. Images were acquired at 675–690  $\mu\text{m}$  below the pia with system AO (**a**) or full AO (**b**) correction using excitation wavelength  $\lambda = 1,030\text{ nm}$ . The SST<sup>+</sup> neurons were labeled with tdTomato. **c**, Signal profiles along the lines in **a** and **b**. **d,e**, Spectral power as a function of spatial frequency  $k$

for the images in **a** and **b**. **f**,  $|k|$ -space plot of the spatial frequency with system AO and full AO correction. **g,h**, Spot patterns on the SHWS (**g**) and reconstructed wavefront phase map on DM (**h**) for correcting the sample aberration in **a**. **i**, Zernike coefficients of the reconstructed wavefront.

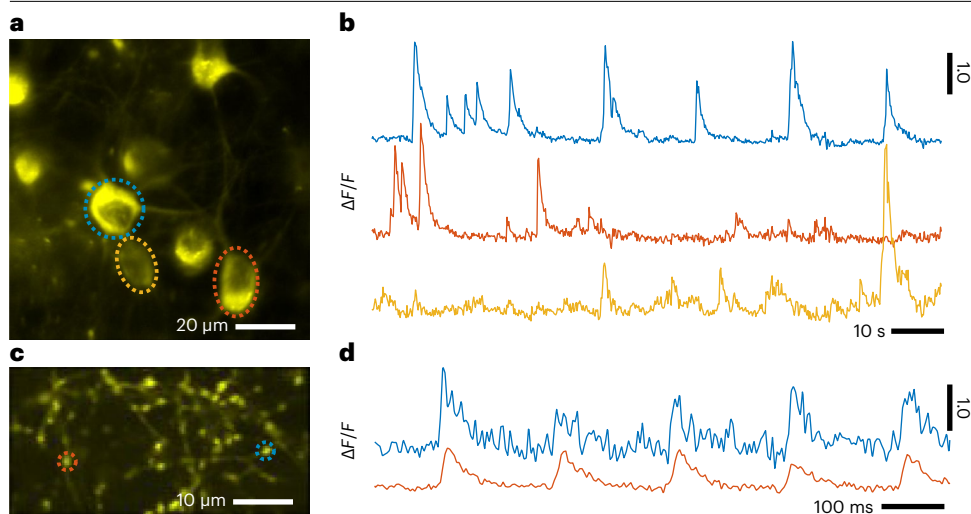


**Fig. 18 | Functional imaging AO correction.** **a**, In vivo two-photon imaging of the layer 5 neurons of vS1 cortex that were labeled with jRGECO1a. Data were obtained at 630 μm below the pia with full AO correction using excitation wavelength  $\lambda = 1,030$  nm. **b**, Calcium signal in the ROIs defined by the dashed circles in **a**. **c**, In vivo two-photon imaging of the thalamocortical boutons that were labeled with iGluSnFR3. Data were obtained at layer 4 of vS1 cortex with full AO correction using excitation wavelength  $\lambda = 970$  nm. **d**, Glutamate dynamics responding to 5 Hz air puff in the ROIs defined by the dashed circles in **c**.

treatment that may be performed for a specific experiment<sup>25,38</sup>. To prevent the incident light cone from being blocked by the edge of the optical window, for deep-layer imaging, we recommend use of a cover glass that is larger than the area of interest.

79. Briefly anesthetize the mice with isoflurane and deliver 50 μL of 3% (wt/vol) solution in saline of Cy5.5–dextran into the lumen of blood vessels via retro-orbital intravenous injection<sup>23</sup>. The Cy5.5–dextran can circulate for more than 4 h in the blood<sup>38</sup> and provide a stable guidestar signal during this period.
80. Start ScanImage. Initialize the DM and load the system aberration correction coefficients to the DM based on your imaging wavelength. Turn on the EMCCD and SOLIS software. Set the temperature as  $-60^{\circ}\text{C}$ . Find the FOV within the window formed by a craniotomy<sup>25</sup> or thinned bone<sup>24,39</sup>.
  - ▲ **CRITICAL STEP** Make sure the cranial window is horizontal, i.e., perpendicular to the optical axis. A tilted window will alter the sample aberration correction such that the FOV is shifted after sample aberration correction.
81. Use dichroic mirror DI' as the main dichroic. Tune the laser to 1,250 nm for Cy5.5 and load the system aberration correction coefficients for 1,250 nm. Image the microvessels in the ROI with the far-red channel.
  - ▲ **CRITICAL STEP** As the tissue aberration varies gradually with changes in the location of the FOV, we recommend the user to perform the sample aberration correction for individual  $100\text{ }\mu\text{m} \times 100\text{ }\mu\text{m}$  FOVs, or  $50\text{ }\mu\text{m} \times 50\text{ }\mu\text{m}$  FOVs; the latter area is a phenomenological limit to the isoplanatic region<sup>16,27</sup>.
82. Replace dichroic mirror DI' with dichroic DI so that the far-red emission light of Cy5.5 is mainly directed to the wavefront sensing path rather than the collection path. Obtain the sample aberration pattern on the SHWS by a long exposure, i.e., 1–30 s depending on the SNR (Fig. 17g). Adjust the EMCCD gain to achieve a good signal of the sample aberration pattern. Save the sample aberration pattern.
  - ▲ **CRITICAL STEP** The SNR of the sample aberration pattern is fundamental to the AO correction. To improve the signal for deep tissue, we recommend use of the ScanImage 'microROI' function. By selecting ROIs on the microvessel, the galvo mirrors will only scan on the vessel during the period of exposure and avoid collecting at times devoid of a signal.



83. Run 'sample aberration correction', which computes the shifts of the center of individual spots in the sample aberration pattern from the reference pattern and decomposes the shifts to the Zernike mode pattern. This determines the coefficients for sample aberration correction (Fig. 17h,i).
84. Add the sample aberration correction coefficients to the system aberration correction coefficients for wavelength that you plan to use and send them to the DM. At this point, both the system aberration as well as the sample aberration for that FOV are corrected. Start the recording (Fig. 17a–c).
 

▲ **CRITICAL STEP** In a successful sample correction, the user should see a substantial increase in signal-to-background ratio (Fig. 17a–c) and spatial resolution, which can be quantified by a two-dimensional fast Fourier transform of images in polar coordinates (Fig. 17d–f).

◆ **TROUBLESHOOTING**
85. If you have another FOV to record, center at the new FOV, and repeat Steps 79–84.

## Troubleshooting

Troubleshooting advice can be found in Table 5.

**Table 5 | Troubleshooting table**

Step	Problem	Possible reason	Solution
11, 25	The expanded beam size is substantially larger than anticipated	In the discussion in Step 11, we made the assumption that the laser output is collimated. However, it is important to note that as a Gaussian beam, the laser output naturally exhibits a slight divergence	To compensate for the divergence of the Gaussian beam, one can adjust the distance between lenses L1 and L2 to achieve a collimated beam at the output of the beam expander, as described in Step 25. Although this adjustment may result in a slight change in the magnification of the beam expander, it can probably be ignored for this particular application since precise control of the output beam size is not a requirement
		Another consequence of the Gaussian beam's divergence is that if we assume the same diameter as the laser output for Beam size <sub>in</sub> , it underestimates the actual beam size. The natural divergence of the Gaussian beam results in a broader beam profile as it propagates. Therefore, taking the laser output diameter as Beam size <sub>in</sub> would lead to an underestimated measurement of the beam size at the input to the beam expander	The optical path from the laser output to the telescope should be minimized to reduce the effect
43	The sharp edge of the DM is not visible on the EMCCD image	The incident beam to the DM is not sufficiently expanded	Measure the size of the beam that is incident to the DM and adjust the collimation and the distance of L1 and L2 as discussed in Steps 11 and 25
		The DM, pupil, and EMCCD are not conjugated to each other	Check the conjugation as described in Steps 38 and 42
	The edge is sharp but not circular in shape	The beam was cropped by something in the optical path, often the pupil mirror or the scanners	Move the pupil mirror horizontally to test if this fixes the problem before checking the alignment of the system
45	The calibration reference pattern and the sample reference pattern cannot be overlapped with each other	Misalignment	Adjust mirrors M6 and M7 to center the laser to the DM
		The objective might introduce aberrations such as spherical aberration to the sample reference pattern	Adjust the correction ring on the objective while acquiring the sample reference pattern until the new pattern best matches the calibration reference pattern. Fix the correction ring at this position for the rest of the procedure
		The excitation beam is not collimated, especially if you see the grid size differs in the two reference patterns	Move stage TS3 along the rail to change the divergence of the emitted light. Then, recollimate the wavefront sensing beam as described in Step 40



Table 5 (continued) | Troubleshooting table

Step	Problem	Possible reason	Solution
48	Random dots and/or small objects present in the EMCCD image are erroneously detected as focused spots	The detection threshold for the focused spots is set too low, leading to the identification of spurious or undesired spots in the image	Adjusting the detection threshold to a more appropriate level can help improve the accuracy and reliability of spot detection. The detection threshold can be adjusted (shstruct.thresh_course_img, line 133) to exclude these spots
	The putative Zernike pattern appears very different from the ideal Zernike modes and there is nothing wrong with the calibration, i.e., no extra spots, perfect overlap of the pupil and DM, and well-aligned wavefront sensing pathway	The DM does not accurately display the Zernike modes as expected. The DM fails to properly represent the desired Zernike patterns	Contact the DM manufacturer to calibrate the DM influence function
84	Image is not improved by the correction	The SNR of the sample aberration pattern is insufficient for accurately estimating the aberrated wavefront	Increase the excitation beam power up to 250 mW
			Extend the exposure time during wavefront sensing
			Increase the EMCCD gain in SOLIS, typically from 2 to 80
			Use ScanImage 'microROI' function to select ROIs on the microvessel
			Use a Zernike mode pattern in which the detected spots are weighted by their SNR when calculating the Zernike coefficients
		The FOV is larger than the isoplanatic patch	Reduce the FOV to 50 $\mu\text{m}$ $\times$ 50 $\mu\text{m}$
		Improper calibration	Check the AO calibration (Steps 43–65)

Timing

- Steps 1–22, Assembly of the AO-TPLSM: 5–10 d  
Steps 23–42, Alignment and conjugation: 10–15 d  
Steps 43–49, AO calibration: 2–5 d  
Steps 50–53, System aberration calibration: 2–5 h  
Steps 54–65, System verification: 2–3 h  
Steps 66–78, Synthesis of guidestar: 2 d  
Steps 79–85, AO-TPLSM imaging: 3–5 h per mouse

Anticipated results

By measuring and correcting the sample aberration, using the AO-TPLSM instrumentation and procedures described above, one can reliably image the deep layers of the mouse cortex *in vivo*. In particular, the tissue aberration in the mouse neocortex is dominated by the low-order Zernike modes (Fig. 17g–i) and thus amenable to correction. Figure 17 shows an example image of the somatostatin positive neurons in layer 5 of the somatosensory cortex, where fine structures such as the neuronal processes can only be resolved after correcting for the sample aberration (Fig. 17a–c). A two-dimensional Fourier transform of the images reveals that AO correction leads to a resolution that approaches the diffraction limit (Fig. 17d–f). For functional imaging, using endogenous expression of the red-shifted calcium indicator jRGECO1a (ref. 4), the signal can approach a signal-to-RMS-noise ratio of 50 in the layer 5b pyramidal neurons with aberration correction (Fig. 18a,b). Further, one can use AO-TPLSM to monitor the endogenous expression of the red-shifted glutamate sensor iGluSnFR3 (ref. 7) to observe synaptic release, as demonstrated for thalamocortical glutamate transmission to layer 4 of neocortex (Fig. 18c). A signal-to-RMS noise ratio that exceeds 5 is achieved after AO correction (Fig. 18d).

As improper calibration is a common cause for poor performance of AO-TPLSM, as described in this protocol, we designed a fiber sample test to evaluate the system before the actual experiment (Steps 54–65). The aberration of this sample is dominated by the spherical aberration (Fig. 15c–e), which is induced by the double-layer cover glass. Typically, the system aberration correction increases the signal for ~20%, whereas the full AO correction usually doubles the signal.

## Data availability

The data used for generating the time series in Figs. 17 and 18 can be accessed via <https://dandiarchive.org/dandiset/000454/0.230302.2331>.

## Code availability

The MATLAB scripts for calibrating and operating the AO-TPLSM are available in the Supplementary Software.

Received: 8 February 2023; Accepted: 24 July 2023;  
Published online: 01 November 2023

## References

- Denk, W., Strickler, J. H. & Webb, W. W. Two-photon laser scanning fluorescence microscopy. *Science* **248**, 73–76 (1990).
- Kleinfeld, D., Mitra, P. P., Helmchen, F. & Denk, W. Fluctuations and stimulus-induced changes in blood flow observed in individual capillaries in layers 2 through 4 of rat neocortex. *Proc. Natl Acad. Sci. USA* **95**, 15741–15746 (1998).
- Svoboda, K., Denk, W., Kleinfeld, D. & Tank, D. W. In vivo dendritic calcium dynamics in neocortical pyramidal neurons. *Nature* **385**, 161–165 (1997).
- Dong, C. et al. Fluorescence imaging of neural activity, neurochemical dynamics, and drug-specific receptor conformation with genetically encoded sensors. *Annu. Rev. Neurosci.* **45**, 273–294 (2022).
- Chen, T. W. et al. Ultrasensitive fluorescent proteins for imaging neuronal activity. *Nature* **499**, 295–300 (2013).
- Marvin, J. S. et al. Stability, affinity, and chromatic variants of the glutamate sensor iGluSnFR. *Nat. Methods* **15**, 936–939 (2018).
- Aggarwal, A. et al. Glutamate indicators with improved activation kinetics and localization for imaging synaptic transmission. *Nat. Methods* **20**, 925–935 (2023).
- Villette, V. et al. Ultrafast two-photon imaging of a high-gain voltage indicator in awake behaving mice. *Cell* **179**, 1590–1608 e23 (2019).
- Kleinfeld, D. et al. Can one concurrently record electrical spikes from every neuron in a mammalian brain? *Neuron* **103**, 1005–1015 (2019).
- Jun, J. J. et al. Fully integrated silicon probes for high-density recording of neural activity. *Nature* **551**, 232–236 (2017).
- Ohki, K., Chung, S., Ch'ng, Y. H., Kara, P. & Reid, R. C. Functional imaging with cellular resolution reveals precise micro-architecture in visual cortex. *Nature* **433**, 597–603 (2005).
- Xu, S. et al. Behavioral state coding by molecularly defined paraventricular hypothalamic cell type ensembles. *Science* **370**, eabb2494 (2020).
- Hampson, K. M. et al. Adaptive optics for high-resolution imaging. *Nat. Rev. Methods Prim.* **1**, 68 (2021).
- Wang, K. et al. Direct wavefront sensing for high-resolution in vivo imaging in scattering tissue. *Nat. Commun.* **6**, 7276 (2015).
- Wang, K. et al. Rapid adaptive optical recovery of optimal resolution over large volumes. *Nat. Methods* **11**, 625–628 (2014).
- Liu, R., Li, Z., Marvin, J. S. & Kleinfeld, D. Direct wavefront sensing enables functional imaging of infragranular axons and spines. *Nat. Methods* **16**, 615–618 (2019).
- Debarre, D. et al. Image-based adaptive optics for two-photon microscopy. *Opt. Lett.* **34**, 2495–2497 (2009).
- Tang, J., Germain, R. N. & Cui, M. Superpenetration optical microscopy by iterative multiphoton adaptive compensation technique. *Proc. Natl Acad. Sci. USA* **109**, 8434–8439 (2012).
- Ji, N., Milkie, D. E. & Betzig, E. Adaptive optics via pupil segmentation for high-resolution imaging in biological tissues. *Nat. Methods* **7**, 141–147 (2010).
- Streich, L. et al. High-resolution structural and functional deep brain imaging using adaptive optics three-photon microscopy. *Nat. Methods* **18**, 1253–1258 (2021).
- Rodriguez, C. et al. An adaptive optics module for deep tissue multiphoton imaging in vivo. *Nat. Methods* **18**, 1259–1264 (2021).
- Aviles-Espinosa, R. et al. Measurement and correction of in vivo sample aberrations employing a nonlinear guide-star in two-photon excited fluorescence microscopy. *Biomed. Opt. Express* **2**, 3135–3149 (2011).
- Yardeni, T., Eckhaus, M., Morris, H. D., Huizing, M. & Hoogstraten-Miller, S. Retro-orbital injections in mice. *Lab Anim. (NY)* **40**, 155–160 (2011).
- Drew, P. J. et al. Chronic optical access through a polished and reinforced thinned skull. *Nat. Methods* **7**, 981–984 (2010).
- Holtmaat, A. et al. Long-term, high-resolution imaging in the mouse neocortex through a chronic cranial window. *Nat. Protoc.* **4**, 1128–1144 (2009).
- Ji, N., Sato, T. R. & Betzig, E. Characterization and adaptive optical correction of aberrations during in vivo imaging in the mouse cortex. *Proc. Natl Acad. Sci. USA* **109**, 22–27 (2012).
- Ji, N. Adaptive optical fluorescence microscopy. *Nat. Methods* **14**, 374–380 (2017).
- Wang, C. et al. Multiplexed aberration measurement for deep tissue imaging in vivo. *Nat. Methods* **11**, 1037–1040 (2014).
- Qin, Z. et al. Adaptive optics two-photon microscopy enables near-diffraction-limited and functional retinal imaging in vivo. *Light Sci. Appl.* **9**, 79 (2020).
- Meng, G. et al. High-throughput synapse-resolving two-photon fluorescence microendoscopy for deep-brain volumetric imaging in vivo. *eLife* **8**, e40805 (2019).
- Resendez, S. L. et al. Visualization of cortical, subcortical and deep brain neural circuit dynamics during naturalistic mammalian behavior with head-mounted microscopes and chronically implanted lenses. *Nat. Protoc.* **11**, 566–597 (2016).
- Qin, Z. et al. Adaptive optics two-photon endomicroscopy enables deep-brain imaging at synaptic resolution over large volumes. *Sci. Adv.* **6**, eabc6521 (2020).
- Noll, R. J. Zernike polynomials and atmospheric-turbulence. *J. Opt. Soc. Am.* **66**, 207–211 (1976).
- Berlage, C. et al. Deep tissue scattering compensation with three-photon F-SHARP. *Optica* **8**, 1613–1619 (2021).
- Papadopoulos, I. N., Jouhanneau, J.-S., Poulet, J. F. A. & Judkewitz, B. Scattering compensation by focus scanning holographic aberration probing (F-SHARP). *Nat. Photonics* **11**, 116–123 (2016).
- Podgorski, K. & Ranganathan, G. Brain heating induced by near-infrared lasers during multiphoton microscopy. *J. Neurophysiol.* **116**, 1012–1023 (2016).
- Prevedel, R. et al. Fast volumetric calcium imaging across multiple cortical layers using sculpted light. *Nat. Methods* **13**, 1021–1028 (2016).
- Shih, A. Y. et al. Two-photon microscopy as a tool to study blood flow and neurovascular coupling in the rodent brain. *J. Cereb. Blood Flow. Metab.* **32**, 1277–1309 (2012).
- Yang, G., Pan, F., Parkhurst, C. N., Grutzendler, J. & Gan, W. B. Thinned-skull cranial window technique for long-term imaging of the cortex in live mice. *Nat. Protoc.* **5**, 201–208 (2010).

## Acknowledgements

We thank S. Adams for assistance with Cy5.5–dextran synthesis and B. Friedman for assistance with animal preparations. This work was funded by the National Science Foundation, grant PHY no. 1532264; the National Institutes of Health, grants U24 EB028942, R35 NS097265 and

U19 NS107466; and Early and Advanced Postdoc Mobility fellowships (P2SKP3\_164948 and P3OOPA\_177804) from the Swiss National Science Foundation.

## Author contributions

D.K. and R.L. guided this project and R.L. and P.Y. designed the microscope, which is based on a prior design by R.L. P.Y. carried out fabrication and testing of the hardware, T.B., R.L. and M.T. developed the method to synthesize the Cy5.5–dextran, R.L. and P.Y. performed all in vivo measurements, and D.K. and P.Y. wrote the manuscript. D.K. attended to the plethora of university rules and forms that govern research compliance, export control and environmental health and safety, including the ethical use of animals as well as the use of chemicals, hazardous substances, controlled substance, lasers and viruses.

## Competing interests

The authors declare no competing interests.

## Additional information

**Supplementary information** The online version contains supplementary material available at <https://doi.org/10.1038/s41596-023-00893-w>.

**Correspondence and requests for materials** should be addressed to David Kleinfeld.

**Peer review information** *Nature Protocols* thanks Valentina Emiliani, Karen Hampson and the other, anonymous, reviewer(s) for their contribution to the peer review of this work.

**Reprints and permissions information** is available at [www.nature.com/reprints](http://www.nature.com/reprints).

**Publisher's note** Springer Nature remains neutral with regard to jurisdictional claims in published maps and institutional affiliations.

Springer Nature or its licensor (e.g. a society or other partner) holds exclusive rights to this article under a publishing agreement with the author(s) or other rightsholder(s); author self-archiving of the accepted manuscript version of this article is solely governed by the terms of such publishing agreement and applicable law.

## Related links

### Key reference using this protocol

Liu, R. et al. *Nat. Methods* **16**, 615–618 (2019): <https://doi.org/10.1038/s41592-019-0434-7>

© Springer Nature Limited 2023